Modelling of Industrial Processes for Polymer Melts:
Extrusion and Injection Moulding

Fons van de Ven

Eindhoven University of Technology
P.O.Box 513; 5600 MB Eindhoven, The Netherlands

Abstract. In this chapter, a survey is presented of the research on polymers performed by a unit of the mathematics faculty of Eindhoven University of Technology (EUT) during the years 1995 to 2000. Special attention is given to the mathematical modelling of industrial processes for polymers. An outline of a set of projects concerned with polymer processes as extrusion, injection moulding, polymer blending, blow moulding, cable coating and fiber spinning is given. Finally, injection moulding between two parallel plates is considered. The mechanical and thermal features of this process are modelled. A project on the instability ('wobbling') of the free flow front is discussed.

1 Introduction to the Research Unit

1.1 Description of the Research Unit

Our research unit is part of the:

> Section: Applied Analysis/Continuum Mechanics.
> Faculty: Mathematics and Computing Science.
> Eindhoven University of Technology (EUT)

Our main activities within the research on polymers is in the mathematical modelling of industrial processes for polymer products, such as; fibers, sheets, compact discs, etc. Examples of these processes are: extrusion, injection moulding, blow moulding and fiber spinning. From the mathematical models we try to derive both analytical and numerical simulations of the processes. These simulations can serve us to suggest ways for improving the processes (better final products, shorter production times). A special point of attention for us is in the investigation of the (in)stability of the processes. Industrial contacts (a.o. for experimental data) are essential in these research topics.

1.2 Members of the Unit

The research unit, as far as research in the field of polymers concerns, consists of:

- Senior academic staff:
    - Dr.A.A.F.van de Ven
    - Dr. J. Molenaar
- PhD:
    - Dr. A.C.T. Aarts (till 1-3-1997)
    - Dr. C.F.J.den Doelder (from 1-11-1996 till 1-6-1999)
    - H.H.J. Gramberg (from 1-9-1998)
    - A.Y. Gunawan (from 1-10-1998 till 31-1-1999, and from 1-2-2000)
    - S.M.P. Smolders (from 1-11-1999)
- Twaio (trainees from Mathematics for Industry):
    - I.I. Ptitchkina (from 1-2-1996 till 1-9-1996)
    - C.F.J. den Doelder (from 1-3-1996 till 1-10-1996)
    - Dr. Y.M.M. Knops (from 1-7-1996 till 1-2-1997)
    - R. Klein Meulenkamp (from 1-2-1998 till 1-9-1998)
    - S.M.P. Smolders (from 1-1-1999 till 1-9-1999)
- MsC-student:
    - R.den Adel (from 1-1-1996 till 1-9-1996)
    - H.H.J. Gramberg (from 1-4-1997 till 1-2-1998)
    - D. Bekers (from 1-4-1998 till 1-2-1999)
    - J. Kroot (from 1-2-1999 till 1-12-1999)
    - V. Lemmen (from 1-3-1999 till 1-12-1999)

Industrial contacts are:

- DOW Benelux, Terneuzen, The Netherlands
- DSM Research, Geleen, The Netherlands
- Axxicon Moulds Eindhoven, The Netherlands

1.3   Overview of Research Topics

The research projects on polymers executed by our group during the last five years can be divided into the following main groups:

1. **Extrusion**
   In extrusion of for instance plastic fibers, flow instabilities can occur, when increasing the rate of production. The distortions due to these instabilities make the final product worthless. So, it is of great importance for industries to know how these instabilities can be prevented, or at least how the critical rate of production can be increased. This can be done by adapting the geometry of the apparatus and/or the constitution of the polymer. In order to find out how this is best achieved, a simulation of the processes under consideration is needed. In two ways, such a simulation is searched for:
   (a) On the basis of a full 3-dimensional theory using a nonlinear viscoelastic constitutive model for the polymer (Aarts, [1]);

(b) On the basis of a 1-dimensional, discrete model incorporating either stick-slip or spurt-flow (Den Doelder, [2]).

Instabilities in extrusion are classified in: sharkskin, spurt and gross melt fracture. The 3-dimensional model showed the existence of persistent periodic oscillations related to flow instabilities. For spurt, a discrete model is constructed, describing relaxation oscillations in good correspondence with experimental results (performed at DOW).

Incorporated Industries
DOW, DSM.
Incorporated staff/students
Van de Ven, Molenaar, Aarts, Den Doelder, Den Adel.
For further results see Sect. 2.

2. **Injection Moulding**
Injection moulding is considered especially with regard to the production of compact discs (CD's). This process shows two different types of problems:

- a 'macroscopic' problem: the filling of the mould;
- a 'microscopic' problem: the filling of the pits.

Relevant effects are the influence of temperature and pressure on the filling of the pits, and that of the elastic properties of the viscoelastic melt on residual stresses and deformations in the CD ($\rightarrow$ PhD-project Smolders).
A specific effect of interest is the so called front instability that can occur in the filling phase of an injection moulding process ($\rightarrow$ PhD-project Gramberg). For this project, see also Sect. 3
Further aspects that have been under study are:

- Modelling and numerical simulation of the temperature and pressure in the filling phase of an injection moulding process.
- Calculation of the temperature distribution on microscopic scale at the pits.
- Thermal shrinkage at microscopic level.

Incorporated Industries
Axxicon, DSM.
Incorporated staff/students
Van de Ven, Gramberg, Klein Meulekamp, Hinterkörner (Leonardo), Smolders, Bekers, Kroot.

Results

(a) Klein Meulekamp, R., The Injection Moulding of Compact Discs, Eindhoven University of Technology, Final report of postgraduate programme Mathematics for Industry, 1999, Eindhoven; *confidential*.

(b) Hinterkörner, R., Injection Moulding of Compact Discs, Report for an industrial placement at Axxicon Moulds, Eindhoven, 1998; *confidential*.

(c) Bekers, D., Microscopic Flow Behaviour in the Injection Moulding of Compact Discs. Master's Thesis, Eindhoven University of Technology, February 1999, Eindhoven; *confidential*.

(d) Smolders, S.M.P., A Viscoelastic Model of the Injection Moulding of Compact Discs. Eindhoven University of Technology, Final report of postgraduate programme Mathematics for Industry, 1999, Eindhoven; *confidential*.

(e) Kroot, J., Shrinkage on Microscopic Level During the Injection Moulding of Compact Discs. Master's Thesis, Eindhoven University of Technology, December 1999, Eindhoven; *confidential*.

3. **Morphology of Polymer Blends**

DSM develops new synthetic materials by blending several polymers. The material properties of a polymer blend are closely connected with the morphology of the blend. This morphology is highly determined by the blending process in an extruder. The material properties can be predicted better, if we obtain a better understanding of these blending processes. The morphology problem concerns the breaking-up of polymer threads immersed in another polymeric fluid. A solution for the breaking-up of two parallel threads is derived. This breaking-up occurs either in-phase or out of phase. The solution predicts when these types of breaking-up occur. This depends on:

- the distance between the threads;
- the viscosity ratio of the two fluids.

The analytical solution found is in agreement with experiments (performed at DSM-Research). This research is continued as a PhD-project (supported by Scientific Cooperation Netherlands-Indonesia) by Gunawan (delegated from:Institut Teknologi Bandung, Indonesia), to start at 1-2-2000.

Incorporated Industries
DSM.
Incorporated staff/students
Van de Ven, Molenaar, Knops, Gunawan.

Results

(a) Knops, Y.M.M., Morphology Developments in Polymer Blends; The Hydrodynamical Interaction between Disintegrating Threads, Final report of postgraduate programme Mathematics for Industry, 1997, Eindhoven; *confidential*.

(b) Gunawan, A.Y., The Breaking-up Process of Two Polymer Threads, Report IWDE 99-04, Eindhoven University of Technology, January 1999, Eindhoven.

4. **Some Smaller Projects**

All of these projects are performed at and supported by DSM-Research, Geleen. DSM-Research constitutes a firm basis for the maintenance and improvement of the company's technological position. In its organisational structure, close working conditions exist between specialists with different backgrounds. One of their functions is to improve existing materials and develop new ones, and to analyse the flow behaviour of polymer melts and blends.

The following projects were considered:

- *Blow moulding modelling: the influence of sag and die swell.*
  Blow moulding is an industrial process in which different hollow products can be made, e.g. bottles, cans, air ducts and so called Car Velocity Joints Boots. In *blow moulding* a polymer melt is forced through an annular die in order to produce a hollow cylindrical tube called a parison. The length of the parison and its thickness distribution are of central importance for the quality of the final product. Two competitive effects are observed, commonly known as *sag* and *swell*. Sag, a time dependent stretching of the extrudate, is caused by gravitational forces. Swell, defined as the increase in cross-sectional area of the extrudate as it comes out of the die, appears due to rearrangement of the velocity profile from die-flow to free-space flow, to elastic properties of the viscoelastic melt, and to temperature effects. Both sag and swell lead to a non-uniform thickness distribution of the parison. To be able to control the shape of the parison, one has to know how the parameters of the geometry, the material and the extrusion process influence sag and swell.
  A simple mathematical model describing the process of parison formation is constructed. The model is developed for two types of fluids: Newtonian and Maxwell, respectively. Analytical results are obtained by use of *Mathematica*. The results are compared with numerical results from the finite element program *Polyflow* and experimental results from DSM.

- *Cable coating: surface instabilities.*
  In a cable coating process, a solid (e.g. copper) wire is covered with a thin shield of polymer (e.g. for electrical insulation). At DSM, surface distortions of a very special kind were observed: these distortions of the extrudate showed up as two sets of spirals running in two directions making angles of approximately 45º with the axis of the wire. The goal of this project was to find a possible explanation for this type of distortions.

- *Fiber spinning: non-uniform elongation and die swell.*
  DSM-Research wants to gain insight in the stretching behaviour of LDPE-polymers during a fiber spinning process. This project aims at the analysis of the melt spinning behaviour of polymer melts in the isothermal melt spinning (Rheotens) test.

In a number of melt processing techniques such as extrusion, coating, film casting and film blowing, the deformation of the polymer melt is governed by elongation. For a rheological characterisation, it is needed to test the materials at very high strain rates. In the so called *Rheotens test* a melt filament is extruded by a capillary rheometer followed by a stretching under nearly isothermal conditions and with increasing draw-down ratio (i.e the ratio between extrusion speed and uptake velocity). This set-up makes it possible to reach high strain rates, but is hampered with non-uniform deformation along the spinline. The Rheotens test gives important information regarding the melt spinning behaviour of a polymer melt. Therefore, a modelling of the Rheotens test is required. This modelling should include

- pre-history in the reservoir, the contraction unit and the die;
- die swell at the exit;
- stretching of the filament.

Incorporated Industries
DSM.
Incorporated staff/students:
Van de Ven, Molenaar, Ptitchkina, Gramberg, Lemmen.

Results

(a) Ptitchkina, I.I., Blow Moulding Modelling, Final report of post-graduate programme Mathematics for Industry, 1996, Eindhoven.
(b) Gramberg, H.H.J., Stability of an Annular Poiseuille Flow, Master's thesis, Eindhoven University of Technology, June 1998, Eindhoven.
(c) Lemmen, V., Analysis of the Isothermal Spinning Behaviour of Polymer Melts. Master's thesis, Eindhoven University of Technology, December 1999, Eindhoven.

2 Flow Instabilities in the Extrusion of Polymer Melts

2.1 Introduction

Extrusion of polymeric melts is employed to produce, e.g., plastic wires, pipes, sheets and plates. The principle of extrusion is that the polymeric melt is forced to flow through a die, e.g., by the action of a driving pressure gradient or a moving piston. In extrusion of plastic fibers flow instabilities can occur when increasing the rate of production. Instabilities in extrusion are classified in: sharkskin, spurt and gross melt fracture. The distortions due to these instabilities make the final product worthless. So, it is of great importance for industries to know how these instabilities can be prevented, or at least how the critical rate of production can be increased. This can be done by adapting the geometry of the apparatus and/or the constitution of the polymer. In

order to find out how this is best achieved, a simulation of the processes under consideration is needed. In two ways, such a simulation is searched for:

1. On the basis of a full 3-dimensional theory using a nonlinear viscoelastic constitutive model for the polymer (constitutive instabilities; Aarts [1]);
2. On the basis of a 1-dimensional, discrete model incorporating either stick-slip or spurt-flow (discrete melt fracture models; Den Doelder [2]).

The 3-dimensional model shows the existence of persistent periodic oscillations related to flow instabilities.
The discrete model describes relaxation or spurt oscillations in good correspondence with experimental results (performed at DOW).

- Incorporated Industries
  DOW, DSM.

2.2 Problem Description

This section deals with the modelling of the extrusion process. The extruder consists of a wide cylindrical barrel connected to a narrow cylindrical capillary; see Fig. 1. Thus, the radius R of the capillary is small compared to the radius R_b of the barrel. The centerlines of the barrel and the capillary coincide. Cylindrical coordinates (r, θ, z) are introduced with the z-axis along the centerline of the extruder, and $z = 0$ corresponding to the position where the barrel is connected to the capillary.
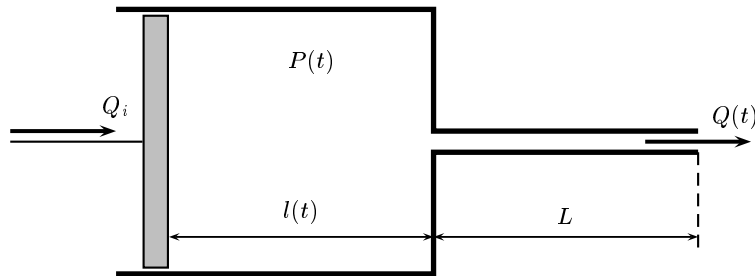
Fig. 1. The extruder which consists of a wide barrel and a narrow cylindrical capillary. The melt in the barrel is compressed by a plunger moving with constant speed V_0 in the positive z-direction

The polymeric melt in the barrel is compressed by a plunger, moving at constant speed V_0 in the positive z-direction. Due to the plunger movement a pressure P is built up inside the barrel, and the melt is forced to leave the barrel at $z = 0$ and to flow into the capillary, with volumetric flow rate Q. At

the end of the capillary, i.e. at $z = L$ where L denotes the capillary length, the melt leaves the capillary and the extrudate is formed. Since the flow in the barrel and in the capillary are of essentially different types, the two flows are also modelled in different ways. In the main part of the barrel the flow is aligned along the z-axis, and the flow is an almost uniform compression flow. The pressure becomes very high here due to the narrow inlet of the capillary, but the velocity is rather low because the barrel is very wide (as compared to the capillary). Hence, in the barrel the flow is compression dominated, and shear is negligible here. Thus, the compressibility of the melt inside the barrel must be taken into account, and the melt density ρ is variable. Since the flow in the barrel is uniform, P and ρ are only time-dependent, i.e. $P = P(t)$ and $\rho = \rho(t)$. On the other hand, the flow in the capillary is strongly shear dominated (due to the no-slip condition at the wall and the relatively high velocity compared to that in the barrel) and then the influence of compressibility is small, and in fact negligible. Therefore, the melt flowing through the capillary is assumed incompressible. Hence, the melt flows through the whole capillary with volumetric flow rate $Q = Q(t)$.

We first consider the flow inside the barrel. Taking into account the global mass balance in the barrel, together with a linearly elastic compressibility law for the pressure, one can derive the following relation between the pressure in the barrel and the volumetric flow rate flowing into the capillary (cf. [3], [4])

$$\frac{dP(t)}{dt} = -\frac{K\left[Q(t) - Q_i\right]}{Al(t)}, \quad t > 0, \tag{1}$$

where K is the compression or bulk modulus of the polymeric melt.

Next we consider the flow in the capillary, where the polymeric melt may be considered incompressible. This flow is governed by the equation of motion, and the incompressibility condition:

$$\nabla \cdot \mathbf{v} = 0, \tag{2}$$

where $\mathbf{v}$ is the fluid velocity.
For the strongly viscous shear flow we consider here the inertia terms in the equations of motion may be neglected. Moreover, body forces are absent here, so the equation of motion reduces to

$$\nabla \cdot \mathcal{T} = 0, \tag{3}$$

where $\mathcal{T}$ is the total stress tensor. With the flow aligned along the z-axis, the flow parameters in the capillary are independent of the axial coordinate z and the azimuthal coordinate θ. Under the condition that the flow starts from rest at time $t = 0$, the velocity takes the form

$$\mathbf{v} = v(r, t)H(t)\mathbf{e}_z, \tag{4}$$

where H is the (Heaviside) step function and $\mathbf{e}_z$ is a unit vector in the positive z-direction. The conservation of mass is now automatically satisfied.

The no-slip boundary condition at the wall of the capillary and the regularity of the velocity at the axis require

$$v(R, t) = 0, \tag{5}$$

and

$$\frac{\partial v}{\partial r}(0, t) = 0, \tag{6}$$

respectively.

The characteristic response of the material to a deformation is described by the constitutive equation for the stress. For viscoelastic fluids with fading memory, the stress depends on the deformation history. If a polymer solution contains a small-molecule solvent, this solvent will generally respond in a viscous manner to any applied force or deformation, separately from the elastic response due to the dissolved polymer. Therefore, it is assumed that the extra stress tensor $\mathcal{S} := \mathcal{T} + p\mathcal{I}$ in the fluid consists of a Newtonian viscous component and an isotropic elastic one, namely

$$\mathcal{S} = 2\eta_s \mathcal{D} + \mathcal{S}_p, \quad \Rightarrow \mathcal{T} = -p\mathcal{I} + 2\eta_s \mathcal{D} + \mathcal{S}_p. \tag{7}$$

Here, p is the pressure, $\mathcal{I}$ the unit tensor, and η_s the solvent viscosity. The rate-of-deformation tensor $\mathcal{D}$ is defined by

$$\mathcal{D} = \frac{1}{2}(\mathcal{L} + \mathcal{L}^T), \qquad \mathcal{L} = \text{grad } \mathbf{v} = \frac{\partial \mathbf{v}}{\partial \mathbf{x}}(\equiv (\nabla \mathbf{v})^T). \tag{8}$$

With (4), we see that the only non-zero components of $\mathcal{L}$ and $\mathcal{D}$ are L_{rz} and $D_{rz} = D_{zr}$, where

$$D_{rz} = D_{zr} = \frac{1}{2}L_{rz} = \frac{1}{2}\frac{\partial v}{\partial r}. \tag{9}$$

The elastic part $\mathcal{S}_p$, which characterizes the polymer contribution, is assumed to be described by the constitutive model (KBKZ or JSO). For the constitutive models we consider, $\mathcal{S}$ is related to $\mathcal{D}$, and then, just as $\mathcal{D}$, $\mathcal{S}_p$ only depends on r and t. In that case the axial component of the equation of motion (87) reads

$$\frac{\partial T_{rz}}{\partial r} + \frac{T_{rz}}{r} - \frac{\partial p}{\partial z} = 0. \tag{10}$$

Since T_{rz} is independent of z, the solution for the pressure p takes the form

$$p(r, z, t) = -f(t)z + p_0(r, t). \tag{11}$$

Here, f is the pressure gradient driving the flow, and p_0 is a further irrelevant pressure term. Coupling between the flow in the capillary and the flow in the barrel is achieved by equating the pressure terms in the barrel and in the capillary at $r = 0$, $z = 0$. We assume that the pressure outside the capillary is at level zero, so that $p(0, L, t) = 0$. Then it follows that

$$P(t) = Lf(t), \quad \Rightarrow \quad f(t) = \frac{P(t)}{L}. \tag{12}$$

Integration of (10) with use of (11) leads to the following expression for the shear stress

$$T_{rz} = \eta_s \frac{\partial v}{\partial r}(r,t) + S_{rz}(r,t) = -\frac{1}{2}rf(t), \quad 0 \le r \le R, \quad t > 0. \qquad (13)$$

Finally, the volumetric flow rate Q in the capillary is defined by

$$Q(t) = 2\pi \int_0^R v(r,t)r\,dr. \qquad (14)$$

2.3   Models for Constitutive Instabilities

The aim of the theory presented in this section is to get a better insight into the relation between the characteristic behaviour of polymeric melts and the flow instabilities.
The results presented here are mainly from the PhD-thesis of Aarts, [1], (performed at EUT):

Analysis of the Flow Instabilities in the Extrusion of Polymeric Melts.

by: A.C.T.Aarts.

In this thesis, especially the flow instability 'spurt' is investigated. Spurt in *pressure-driven flows* is experimentally observed through a substantial increase of the volumetric flow rate at a slight increase of the pressure gradient beyond a critical value, while spurt in *piston-driven flows* is accompanied by persistent oscillations in the pressure.

Spurt is explained here in terms of constitutive instabilities (mechanical failure of the polymeric fluid itself), while the no-slip boundary condition at the wall of the die is maintained. The explanation is based on balance laws combined with either of two constitutive models: (1) KBKZ or (2) JSO. To account for the response of a small-molecule solvent, an extra Newtonian viscous term is added to the constitutive model employed.

Pressure-driven Extrusion

For a pressure-driven flow of a KBKZ-fluid through a cylindrical capillary, the occurrence of spurt is demonstrated. It is shown that the steady state solution is not unique if the steady state pressure gradient exceeds a critical value. The asymptotic stability of the possible steady states is established. Numerical computations determine which specific steady state the fluid attains. Phenomena like shape memory and hysteresis are explained (see also [5] and [6]).

The axisymmetric laminar flow of an incompressible fluid through a cylindrical tube, radius R, is considered. The flow starts from rest at $t = 0$, driven

by a prescribed constant pressure gradient $\overline{f}$. Under the neglect of inertia forces the balance of linear momentum for the shear stress T_{rz} yields (see (13))

$$T_{rz} = -\frac{1}{2}r\overline{f}. \qquad (15)$$

The characteristic response of the material is described by a constitutive equation for $\mathcal{S}_p$ according to the KBKZ-model. The total shear stress T_{rz} is given by

$$T_{rz}(r,t) = \eta_s \frac{\partial v}{\partial r}(r,t) - \mu\lambda \int_{-\infty}^{t} \frac{\gamma(r,t,\tau)}{c + 3 + \gamma^2(r,t,\tau)} e^{-\lambda(t-\tau)}d\tau, \qquad (16)$$

where η_s is the solvent viscosity, μ and c are elastic constants and λ is the relaxation rate. The shear strain γ is defined by

$$\gamma(r,t,\tau) = \Gamma(r,t) - \Gamma(r,\tau), \quad \text{where} \quad \Gamma(r,t) = -\int_0^t \frac{\partial v}{\partial r}(r,s)ds. \qquad (17)$$

After the substitution of (16) into (15) and making the resulting equation dimensionless, we arrive at the following integrodifferential equation for $\Gamma(r,t)$

$$\varepsilon\frac{\partial\Gamma}{\partial t}(r,t) + h(\Gamma(r,t))e^{-t} + \int_0^t h(\gamma(r,t,\tau))e^{-(t-\tau)}d\tau = \frac{1}{2}r\overline{f}, \qquad (18)$$

where the function h is defined by $h(x) = x/(1 + x^2)$. Once $\Gamma(r,t)$ for each radial coordinate $r\epsilon[0,1]$ is solved from (18), the (dimensionless) volumetric flow rate $Q(t)$ can be calculated from (14)

$$Q(t) = \int_0^1 r^2 \frac{\partial\Gamma}{\partial t}(r,t)dr. \qquad (19)$$

The latter result is derived after one integration by parts with the aid of the no-slip condition (5) and the definition (17).

Steady state flow The steady state velocity gradient, defined by

$$\omega(r) = \lim_{t\to\infty} -\frac{\partial v}{\partial r}(r,t), \qquad \omega(0) = 0, \qquad (20)$$

satisfies the steady state equation (for each $r\epsilon[0,1]$)

$$\mathcal{F}(\omega(r)) := \varepsilon\omega(r) + \int_0^{\infty} h(\omega(r)s)e^{-s}ds = \frac{1}{2}r\overline{f} =: F(r). \qquad (21)$$

For $0 < \varepsilon < 0.0289$ the function $\mathcal{F}(\omega)$ is nonmonotonous (see Fig. 2). In that case equation (21) has three solutions if $F_m < F < F_M$. Stability analysis reveals that the steady state in which $\omega_M < \omega < \omega_m$ is unstable, whereas the

other two, $\omega < \omega_M$ and $\omega > \omega_m$, are asymptotically stable. If $\overline{f} > \overline{f}_{\mathrm{crit}} :=$ $2F_M$ (supercritical flow) then ω suffers a jump; if $0 \le r < r_M := 2F_M/\overline{f}$ then $0 \le \omega(r) < \omega_M$, whereas if $r_M < r \le 1$ then $\omega(r) > \tilde{\omega}_M (> \omega_M)$ (see Fig. 2). Hence, the velocity gradient has a jump at $r = r_M$, resulting in a kink in the steady state velocity profile $\overline{v}(r)$, as shown in Fig. 2. This phenomenon is called *spurt*.
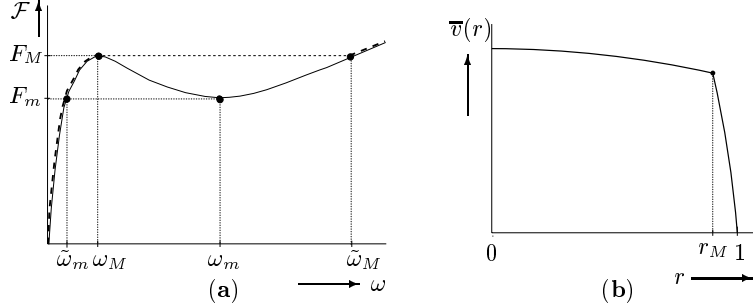

Fig. 2. The function $\mathcal{F}(\omega)$ if $0 < \varepsilon < 0.0289$. The *dashed line* represents the possible ω-solution in supercritical flow (**a**), resulting in a steady state velocity profile, where the spurt layer is located in $r_M \le r \le 1$ (**b**)

In the spurt layer (i.e. $r_M \le r \le 1$) the magnitude of the velocity gradient is very large, in fact

$$\omega(r) = \frac{\overline{f}r}{2\varepsilon}\left[1 - \frac{4\varepsilon}{(\overline{f}r)^2}\log(\frac{\overline{f}r}{2\varepsilon}) + O(\varepsilon)\right], \quad \varepsilon \to 0. \tag{22}$$

These enormous shearing rates near the wall give rise to a dramatic increase in the stationary volumetric flow rate $\overline{Q} := \lim_{t\to\infty} Q(t)$ if the pressure gradient $\overline{f}$ exceeds the critical value $\overline{f}_{\mathrm{crit}}$ (see also Fig. 3).

Loading and unloading; hysteresis and shape memory Consider an experiment in which the flow is initially in a steady state, corresponding to a forcing $\overline{f}_0$, and the forcing is suddenly changed to $\overline{f} = \overline{f}_0 + \Delta\overline{f}$. If $\Delta\overline{f} > 0$ we call this process *loading* and if $\Delta\overline{f} < 0$ *unloading*. Which steady state eventually will be reached after the forcing is changed, depends on the initial state $\overline{f}_0$ and follows from numerical calculations performed on the integrodifferential equation (18). If the load is gradually increased from $\overline{f} = 0$ up to $\overline{f} = \overline{f}_{\mathrm{crit}} = 2F_M$ (subcritical flow) the entire flow is classical: The velocity gradient satisfies $\omega(r) < \omega_M$ and is continuous in r for all $r\epsilon[0, 1]$. As soon as $\overline{f} > \overline{f}_{\mathrm{crit}}$ (supercritical flow) a kink in the velocity profile at $r = r_M = \overline{f}_{\mathrm{crit}}/\overline{f}$ turns up and spurt occurs. This spurt causes an enormous increase of the volumetric rate $\overline{Q}$, as depicted in Fig. 3 (trajectory BC). Let the loading trajectory finish at $\overline{f} = \overline{f}_{\max} (> \overline{f}_{\mathrm{crit}})$; the spurt layer $r^* \le r \le 1$,

where $r^* = \overline{f}_{\mathrm{crit}}/\overline{f}_{\max}$, is of maximum thickness then. From this point the unloading is started. At first the spurt layer remains fixed between $r = r^*$ and $r = 1$. This phenomenon is called *shape memory* (trajectory CD in Fig. 3). During this unloading the magnitude of the shear stress $|T_{rz}| = F$ at r^* decreases according to $F^* := F(r^*) = r^*\overline{f}/2$. If F^* falls below F_m, that is if $\overline{f} < (F_m/F_M)\overline{f}_{\max}$, the boundary $r = r_m := 2F_m/\overline{f}$ of the spurt layer moves back to the wall for further decreasing $\overline{f}$ (trajectory DE in Fig. 3). The spurt layer disappears for $\overline{f} = 2F_m$ and in the final unloading path EA the flow is classical again. The phenomenon that no part of the loading curve in Fig. 3 is retraced until the flow has become entirely classical again, is typical for the occurrence of *hysteresis* in this process.
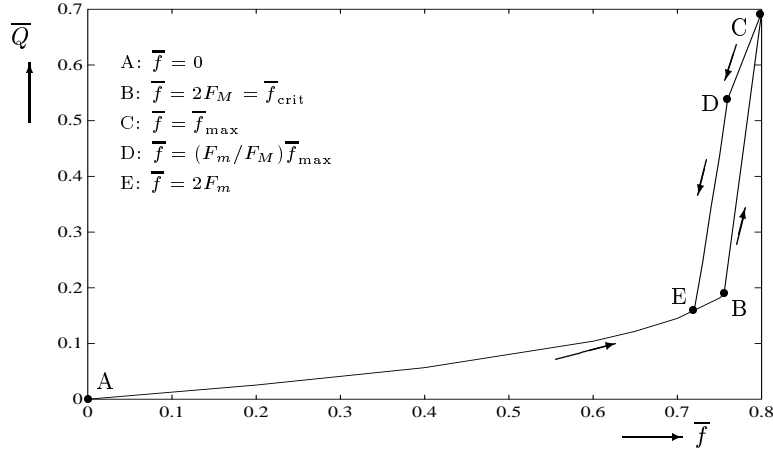
Fig. 3. The flow rate $\overline{Q}$ as function of the forcing $\overline{f}$ in a loading-unloading process. AB: subcritical loading (classical flow), BC: supercritical loading (with thickening spurt layer); CD unloading under shape memory; DE unloading with diminishing spurt layer; EA: subcritical unloading (classical flow)

Newtonian, latency and spurt phase In computing the time dependent velocity gradient, we observe distinct time phases before the steady state is reached. These phases are clearly distinguishable in a (S, N)-plane, where S is defined by (see (18))

$$S(r, t) = h(\Gamma(r, t))e^{-t} + \int_0^t h(\gamma(r, t, \tau))e^{-(t-\tau)}d\tau, \qquad (23)$$

and N, which corresponds to the first normal stress difference $T_{zz} - T_{rr}$, is defined by

$$N(r,t) = g(\Gamma(r,t))e^{-t} + \int_0^t g(\gamma(r,t,\tau))e^{-(t-\tau)}d\tau, \qquad (24)$$

where $g(\gamma) = \gamma h(\gamma)$. From (18) with (21) it follows that

$$S(r,t) = F(r) + \varepsilon \frac{\partial v}{\partial r}(r,t). \qquad (25)$$

For $t \to \infty$ these two functions tend to their stationary values $\overline{S}(r) = J(\omega(r))$ and $\overline{N}(r) = 1 - L(\omega(r))$, where $\omega(r)$ is a solution of (21) and

$$J(\omega) = \int_0^\infty h(\omega s)e^{-s}ds \quad \text{and} \quad L(\omega) = 1 - \int_0^\infty g(\omega s)e^{-s}ds. \qquad (26)$$

According to (21), $\overline{S} = F - \varepsilon\omega$, implying that

$$\overline{N} = 1 - L(\frac{F - \overline{S}}{\varepsilon}). \qquad (27)$$

For a supercritical flow such that $F > F_M$, there exist three distinct time phases; an initial phase, a pseudo steady state and the *spurt phase* in which the flow becomes stationary. At $t = 0$, $S = N = 0$ and $\partial v/\partial r = -F/\varepsilon$. Hence, the solution starts in the origin of the (S,N)-plane and changes on an $O(\varepsilon)$-time scale until $S = F + O(\varepsilon)$. The period of time during which this occurs is referred to as the *Newtonian phase* $(0 \le t < t_N)$. During this phase the following relation holds

$$N = \frac{1}{2}(1 - \sqrt{1 - 4S^2}) + O(\varepsilon), \quad \varepsilon \to 0. \qquad (28)$$

At $t = t_N$ the velocity gradient $\partial v/\partial r$ has become $O(1)$, and this remains so for some time $t > t_N$. Then (25) implies that $S = F + O(\varepsilon)$ and hence S is almost constant. This pseudo steady state that precedes spurt is called the *latency phase*. During this phase, N steadily increases until it is sufficiently close to the line $N = 1 - L((F - S)/\varepsilon)$. After that point, S suddenly decreases and spurt ensues, until the steady state $(\overline{S}, \overline{N})$ is reached. Asymptotics for small ε reveal that the stationary values in the spurt phase satisfy (cf. [6])

$$\overline{S} = \frac{\varepsilon}{F}\log\frac{F}{\varepsilon} - \frac{\varepsilon C}{F} + o(\varepsilon), \qquad \overline{N} = 1 - \frac{\varepsilon\pi}{2F} + O(\varepsilon^2\log\varepsilon), \qquad (29)$$

where $C = 0.57721...$ is Euler's constant.

Conclusions The KBKZ -model supplied with an extra viscous term has been used to describe the flow of a viscoelastic polymeric fluid through a

capillary of an extruder. Internal material properties of the fluid itself account here for the spurt phenomenon and not a global external effect as wall slip. In this section only the flow in the capillary is described. A formulation, in which also the process in the barrel (from which the polymer melt is extrudated into the capillary) is considered, is presented in the next section.

Piston-driven Extrusion

For a piston-driven flow of a JSO-fluid through a cylindrical capillary, spurt accompanied by persistent oscillations in the pressure gradient is found for a bounded range of prescribed flow rates. The influence of compression on the onset of spurt is investigated for an extrusion process that is modelled by the flow of a JSO-fluid through a contraction from a wide barrel into a narrow cylindrical capillary. The fluid in the barrel is compressed by a moving plunger. Numerical computations disclose that persistent oscillations in the pressure as well as in the volumetric flow rate occur for a bounded range of prescribed plunger speeds (see also [1] or [6]).

The elastic part $\mathcal{S}_p$ is described by the constitutive JSO-model. In the JSO-model, $\mathcal{S}_p$ is determined by the following nonlinear differential equation (see Tanner [7, p. 207]):

$$\frac{\mathrm{d}\mathcal{S}_p}{\mathrm{d}t} - \mathcal{L}\mathcal{S}_p - \mathcal{S}_p\mathcal{L}^T + (1-a)(\mathcal{D}\mathcal{S}_p + \mathcal{S}_p\mathcal{D}) + \lambda\mathcal{S}_p = 2\mu\mathcal{D}, \qquad (30)$$

where $\mathrm{d}/\mathrm{d}t$ denotes the material derivative. The relaxation rate λ, the slip parameter $a \in (-1,1)$, and the shear modulus μ are material parameters.

With the velocity given by (4), $L_{zr} = \partial v/\partial r$ is the only non-zero component of $\mathcal{L}$ and the components S_{ij} of $\mathcal{S}_p$ are functions of r and t only. As a result, the material derivative $\mathrm{d}\mathcal{S}_p/\mathrm{d}t$ is equal to the partial time derivative $\partial\mathcal{S}_p/\partial t$, and the components $S_{r\theta}, S_{\theta\theta}$ and $S_{\theta z}$ are identically zero here. Then, the JSO-model transforms into the following equations:

$$\frac{\partial S_{rr}}{\partial t} + (1-a)S_{rz}\frac{\partial v}{\partial r} + \lambda S_{rr} = 0,$$

$$\frac{\partial S_{zz}}{\partial t} - (1+a)S_{rz}\frac{\partial v}{\partial r} + \lambda S_{zz} = 0, \qquad (31)$$

$$\frac{\partial S_{rz}}{\partial t} - \tfrac{1}{2}(1+a)S_{rr}\frac{\partial v}{\partial r} + \tfrac{1}{2}(1-a)S_{zz}\frac{\partial v}{\partial r} + \lambda S_{rz} = \mu\frac{\partial v}{\partial r}.$$

From the first two equations of (31) it follows that $(1+a)S_{rr} + (1-a)S_{zz} = 0$. Introduction of the new variables

$$S := -S_{rz}, \qquad\qquad Z := (1+a)S_{rr} = -(1-a)S_{zz} , \qquad (32)$$

in (31) yields for S and Z the differential equations

$$\frac{\partial Z}{\partial t} - (1 - a^2) S \frac{\partial v}{\partial r} + \lambda Z = 0,$$

$$\frac{\partial S}{\partial t} + Z \frac{\partial v}{\partial r} + \lambda S = -\mu \frac{\partial v}{\partial r}. \tag{33}$$

In terms of S and Z, the stress components T_{ij} of $\mathcal{T}$ according to (7) become

$$T_{rr} = -p + \frac{1}{1+a} Z(r, t), \qquad\qquad T_{\theta\theta} = -p,$$

$$T_{zz} = -p - \frac{1}{1-a} Z(r, t), \qquad\qquad T_{rz} = \eta_s \frac{\partial v}{\partial r}(r, t) - S(r, t), \tag{34}$$

$$T_{r\theta} = T_{\theta z} = 0,$$

where $p = p(r, z, t)$. The first and second normal stress difference $N_1 := T_{zz} - T_{rr}$, and $N_2 := -T_{\theta\theta} + T_{rr}$ are determined by

$$N_1 = -\frac{2}{1-a^2} Z(r, t), \qquad\qquad \frac{N_2}{N_1} = -\frac{1-a}{2}. \tag{35}$$

Hence, Z is related to the first normal stress difference, and the ratio of the two normal stress differences is constant.

The equations describing the extrusion process are made dimensionless by appropriate scaling. Then (1), governing the flow in the barrel, transforms into its dimensionless form:

$$\frac{dP(t)}{dt} = -\frac{1}{\chi} \frac{Q(t) - Q_i}{l(t)}, \quad t > 0, \tag{36}$$

where the dimensionless parameter χ is given by

$$\chi = \frac{8 A l_0 \mu L}{K \pi R^4}. \tag{37}$$

Furthermore, (12) transforms into its dimensionless form

$$f(t) = 8P(t). \tag{38}$$

Equations (33) and (13), governing the flow in the capillary, transform into

$$\frac{\partial S}{\partial t} = -S + w(1 + Z), \qquad \frac{\partial Z}{\partial t} = -Z - wS, \qquad 0 \le r \le 1, \quad t > 0, \tag{39}$$

and

$$\varepsilon w(r, t) + S(r, t) = \frac{1}{2} r f(t), \qquad 0 \le r \le 1, \quad t \ge 0. \tag{40}$$

Here, the velocity gradient, or shear rate, w is defined by

$$w(r,t) = -\frac{\partial v}{\partial r}(r,t), \tag{41}$$

and the dimensionless parameter ε is given by

$$\varepsilon = \frac{\eta_s \lambda}{\mu}. \tag{42}$$

Finally, the volumetric flow rate passes into its dimensionless form

$$Q(t) = 2\int_0^1 v(r,t)r\,dr. \tag{43}$$

The boundary conditions (5) and (6) read in dimensionless form

$$v(1,t) = 0, \qquad w(0,t) = 0, \qquad t > 0. \tag{44}$$

After one integration by parts with the aid of the no-slip boundary condition at the wall, the volumetric flow rate Q can be expressed in terms of the velocity gradient w by

$$Q(t) = \int_0^1 r^2 w(r,t)\,dr. \tag{45}$$

Elimination of w by means of (40), transforms (45) into the following (implicit) relation between the pressure P and the volumetric flow rate Q:

$$P(t) = \varepsilon Q(t) + \int_0^1 r^2 S(r,t)\,dr. \tag{46}$$

Thus, the extrusion process driven by a plunger moving at constant speed, is described by the following system of equations:

$$\frac{\partial S}{\partial t} = -S + w(1+Z), \qquad\qquad \frac{\partial Z}{\partial t} = -Z - wS,$$

$$\varepsilon w(r,t) + S(r,t) = 4rP(t), \qquad P(t) = \varepsilon Q(t) + \int_0^1 r^2 S(r,t)\,dr, \tag{47}$$

$$\frac{dP(t)}{dt} = -\frac{1}{\chi}[Q(t) - Q_i], \qquad 0 \le r \le 1, \quad t > 0.$$

For $t < 0$ the fluid is at rest, and at $t = 0$ the flow is suddenly started up by letting the plunger move at constant speed V_0. The plunger movement induces the constant inlet flow rate Q_i. The initial conditions for P, S and Z, which are supposed to be continuous at $t = 0$, are given by

$$P(0) = 0, \qquad S(r,0) = 0, \qquad Z(r,0) = 0, \qquad 0 \le r \le 1. \tag{48}$$

Substitution of (48) into (47) yields the initial values

$$Q(0) = 0, \qquad w(r,0) = 0, \qquad 0 \le r \le 1. \tag{49}$$

Equations (47), governing the flow in the extruder, can be viewed as a continuous family of quadratic ordinary differential equations coupled by the non-local constraint that determines the flow rate, and the non-local ordinary differential equation that describes the compression in the barrel. The material parameters of the polymeric melt, the plunger speed V_0, and the dimensions of the extruder are included in the three dimensionless parameters ε, χ and Q_i. Notice that ε contains only the material parameters of the polymeric melt, whereas Q_i and χ depend on both the material parameters and the geometry of the extruder. The parameter χ is proportional to the melt compressibility $1/K$.

Steady state flow In this section we investigate the steady state reached by the flow as $t \to \infty$. The steady state flow, driven by the constant inlet flow rate Q_i, is described in terms of the steady state variables

$$\overline{P} = \lim_{t\to\infty} P(t), \qquad \overline{f} = \lim_{t\to\infty} f(t), \qquad \overline{Q} = \lim_{t\to\infty} Q(t),$$
$$\omega(r) = \lim_{t\to\infty} w(r,t), \qquad \overline{S}(r) = \lim_{t\to\infty} S(r,t), \qquad \overline{Z}(r) = \lim_{t\to\infty} Z(r,t), \tag{50}$$

under the assumption that these limits exist. For $t \to \infty$, the equations (38) and (47) reduce to

$$0 = -\overline{S} + \omega(1 + \overline{Z}), \qquad 0 = -\overline{Z} - \omega\overline{S}, \qquad \overline{Q} - Q_i = 0,$$
$$\varepsilon\omega(r) + \overline{S}(r) = 4r\overline{P}, \qquad \overline{P} = \varepsilon\overline{Q} + \int_0^1 r^2\overline{S}(r)dr, \qquad \overline{f} = 8\overline{P}. \tag{51}$$

Hence, $\overline{Q} = Q_i$ and the solutions of $(51)^{1,2}$ expressed in terms of ω read

$$\overline{S}(r) = \frac{\omega(r)}{1 + \omega^2(r)}, \qquad \overline{Z}(r) = -\frac{\omega^2(r)}{1 + \omega^2(r)}. \tag{52}$$

On substitution of $(52)^1$ into $(51)^4$, we find that the steady state velocity gradient can be determined for each $r \in [0,1]$ by solving $\omega = \omega(r)$ from the equation

$$\mathcal{F}(\omega(r)) = F(r), \tag{53}$$

where the steady state shear stress F is defined by

$$F(r) = 4r\overline{P} = \frac{1}{2}r\overline{f}, \tag{54}$$

and the function $\mathcal{F}$ is defined by

$$\mathcal{F}(\omega) = \varepsilon\omega + \frac{\omega}{1 + \omega^2}. \tag{55}$$

For a given inlet flow rate Q_i, the velocity gradient ω must satisfy the constraint

$$Q_i = \int_0^1 r^2 \omega(r) dr, \tag{56}$$

obtained by letting $t \to \infty$ in (45). The steady state velocity profile $\overline{v}(r)$ is obtained by integration of $\overline{v}'(r) = -\omega(r)$ using the boundary condition $\overline{v}(1) = 0$ at the wall.

For $\varepsilon < 1/8$ the function $\mathcal{F}$ is nonmonotone in ω. In Fig. 4 the function $\mathcal{F}(\omega)$ is plotted for a specific value of ε with $0 < \varepsilon < 1/8$. Since the Newtonian viscosity η_s is small in comparison to the shear viscosity μ/λ, we will henceforth assume that $0 < \varepsilon = \eta_s \lambda/\mu < 1/8$.
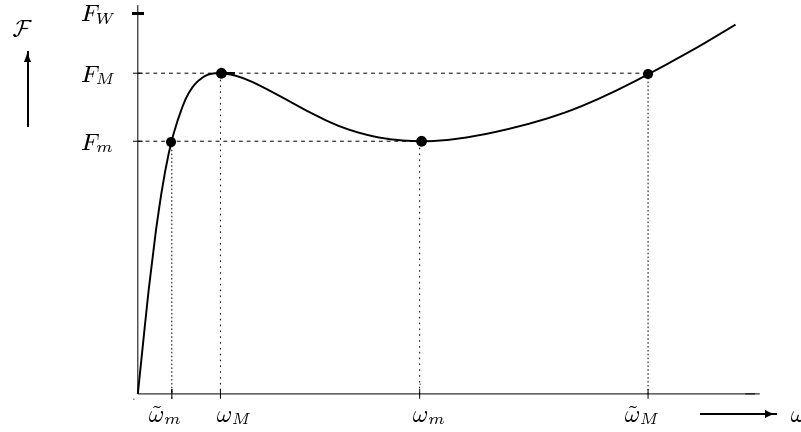

Fig. 4. The function $\mathcal{F}(\omega) = \varepsilon\omega + \omega/(1 + \omega^2)$, when $0 < \varepsilon < 1/8$. In steady state flow the velocity gradient ω satisfies $\mathcal{F}(\omega) = F$, where $F = 4r\overline{P}$ is the steady state shear stress

The steady state shear stress F is linear in r and has its maximum at the wall $r = 1$. If this maximum, denoted by $F_W = 4\overline{P}$, remains below the minimum F_m, then (53) has a unique solution $\omega(r) < \tilde{\omega}_m$ for each radial coordinate r. Clearly, $\omega(r)$ is continuous in r, leading to a smooth steady state velocity profile $\overline{v}(r)$, and the flow is referred to as classical. If the maximum $F_W = 4\overline{P}$ exceeds the minimum F_m, equation (53) has

- one solution if $0 \le F < F_m$;
- three solutions if $F_m < F < F_M$;
- one solution if $F_M < F \le F_W$.

If $F(1) > F_M$, i.e. if $\overline{P} > F_M/4 =: \overline{P}_{crit}$ (supercritical), the steady state velocity gradient $\omega(r)$ has at least one jump at some radial coordinate r. In case of exactly one jump we denote the radial coordinate at which the jump

occurs by r^* ($r^* < 1$), and we refer to the flow as spurt flow. Hence, in spurt flow $\omega(r) < \omega_-^*$ for $0 \leq r < r^*$, whereas $\omega(r) > \omega_+^*$ for $r^* < r \leq 1$, with $\omega_-^* \leq \omega_M$ and $\omega_+^* \geq \omega_m$. The jump in ω results in a kink in the steady state velocity profile $\overline{v}(r)$ at $r = r^*$, and a spurt layer with large velocity gradients forms near the wall.

   In conclusion, for a prescribed constant inlet flow rate Q_i we have for a possible steady state:

- If $0 \leq Q_i \leq \overline{Q}_0$, the steady state is unique; classical flow occurs .

- If $\overline{Q}_0 < Q_i \leq \overline{Q}_{crit}$, the steady state is not unique; either classical flow or spurt flow occurs.

- If $Q_i > \overline{Q}_{crit}$, the steady state is not unique; spurt flow occurs.

Notice that the results derived in this section are only valid in case the steady state does indeed exist.Results of numerical computations as presented in the next section will show whether or not the flow tends to a steady state as $t \to \infty$.

Transient flow behaviour In this section we compute for $t > 0$ the transient/indexflow!transient—(flow, starting from rest at time $t = 0$ and driven by the constant inlet flow rate Q_i due to the plunger movement. The flow is governed by the system of equations (47), with initial conditions (48) and (49). From the numerical results we infer whether the flow reaches a steady state, and we determine the steady state variables. The main interest goes to the relationship between Q_i and the steady state pressure $\overline{P}$. In the case of a classical steady state this relationship is one-to-one ,whereas in the case of a spurt steady state, $\overline{P}$ is not uniquely determined by just Q_i. Whether the flow tends to a steady state, is found to depend on the values of Q_i and the dimensionless parameters ε and χ. For example, for $\varepsilon = 0.005$, in case $\chi = 1$ or $\chi = 2$ we find a range of Q_i-values for which the flow shows so-called persistent oscillations that do not die out, so that no steady state is attained. For $\varepsilon = 0.02$, $\chi = 1$ and $Q_i = 0.1$ (subcritical flow) we observe that $P(t)$ and $Q(t)$ are monotone and smooth functions of t. After sufficient time the flow reaches a classical steady state with a continuous steady state velocity gradient.

   To investigate supercritical flow ($Q_i > \overline{Q}_{crit} = 0.1714$) for $\varepsilon = 0.02$ and $\chi = 1$, we take $Q_i = 0.6$. In Fig. 5, the pressure $P(t)$ and the volumetric flow rate $Q(t)$ are plotted as functions of time t. We observe that oscillations in $P(t)$ and $Q(t)$ appear. These oscillations die out and after sufficient time a steady state is reached. The computations for $Q_i = 0.6$ reveal that the steady state shows a discontinuous velocity gradient $\omega(r)$ with exactly one jump. To investigate whether for $\varepsilon = 0.02$, $\chi = 1$ and a given flow rate Q_i the flow starting from rest reaches a steady state, we compute the transient flow for several flow rates, varying from $Q_i = 0$ to $Q_i = 4.0$. The result is that for all
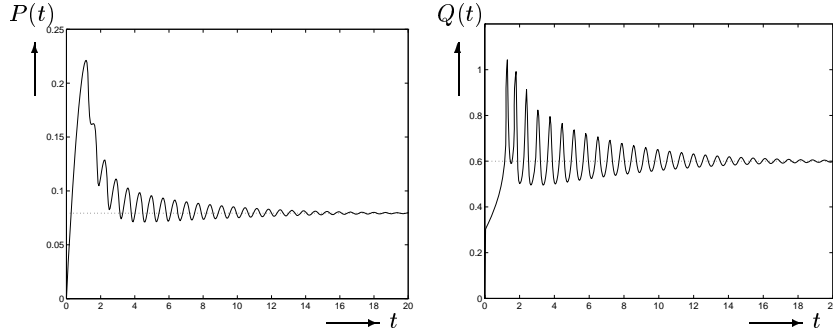
Fig. 5. The pressure $P(t)$ and the volumetric flow rate $Q(t)$ as functions of time t, for $\varepsilon = 0.02$, $\chi = 1$ and $Q_i = 0.6$. The *dotted lines* correspond to the steady state values

values of Q_i considered, a steady state is reached. In Fig. 6a. the steady state pressure $\overline{P}$ attained is plotted versus Q_i, for $\varepsilon = 0.02$ and $\chi = 1$; the plot is drawn as a solid curve. The $\overline{P}$ versus Q_i curve is called the *flow curve*. The flow curve shows a kink at $Q_i = \overline{Q}_{crit}$ and is S-shaped.
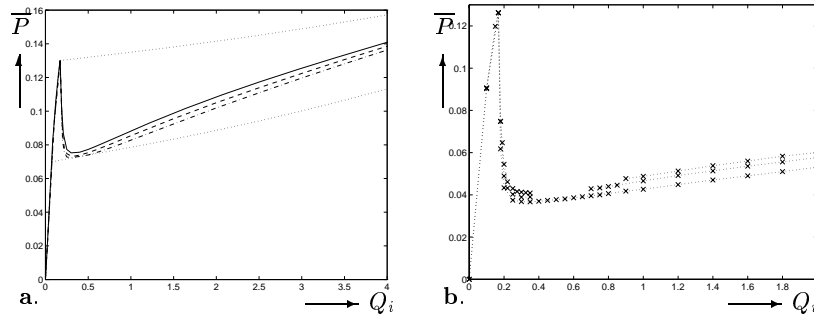

Fig. 6. The flow curves of the steady state pressure $\overline{P}$ versus the inlet flow rate Q_i, for: **a.** $\varepsilon = 0.02$ and $\chi = 1$ (*solid curve*), $\chi = 2$ (*dashed curve*) and $\chi = 4$ (*dashed-dotted curve*). The dotted curves correspond to $\overline{P} = P_{clas}(Q_i)$ (classical flow), $\overline{P} = P_{bottom}(Q_i)$ (bottom-jumping) and $\overline{P} = P_{top}(Q_i)$ (top-jumping). The flow curves show a kink at $Q_i = \overline{Q}_{crit} = 0.1714$, and: **b.** $\varepsilon = 0.005$ and $\chi = 1$, 2, 6. The points $(Q_i, \overline{P})$ marked by the crosses ($\times$) correspond to computed steady states. The gaps in the flow curves for $\chi = 1$ and $\chi = 2$ correspond to flow rates Q_i for which persistent oscillations occur

To investigate the influence of the parameter χ, we compute the transient flow for $\chi = 2$ and $\chi = 4$, keeping $\varepsilon = 0.02$, and we compare the numerical results to those obtained in the case $\chi = 1$, $\varepsilon = 0.02$. The numerical computations disclose that for all values of Q_i considered, a steady state is reached.

In Fig. 6a. the flow curves are plotted for $\varepsilon = 0.02$ and $\chi = 2$ (dashed curve), and for $\varepsilon = 0.02$ and $\chi = 4$ (dashed-dotted curve). We observe that the flow curves for $\chi = 2$ and $\chi = 4$ are S-shaped, just like the flow curve for $\chi = 1$. Furthermore, the flow curves show a kink at $Q_i = \overline{Q}_{crit}$ independent of χ. Notice that for $Q_i < \overline{Q}_{crit}$ the three flow curves for $\chi = 1$, 2 and 4 coincide, whereas at a fixed supercritical flow rate $Q_i > \overline{Q}_{crit}$, the steady state pressure $\overline{P}$ becomes smaller if χ is changed from $\chi = 1$ to the larger values $\chi = 2$ or $\chi = 4$.

Next, we investigate the influence of the parameters ε and χ on the transient flow behaviour and the steady state values attained. To that end, we compute the transient flow for several values of Q_i, when $\varepsilon = 0.005$ and $\chi = 1$, 2 and 6. In Fig. 7, Fig. 8 and Fig. 9 the pressure $P(t)$ and the volumetric flow rate $Q(t)$ are plotted as functions of time t, for $\varepsilon = 0.005$, $\chi = 1$, and $Q_i = 0.2$, 0.6 and 2.0, respectively. We observe that oscillations in $Q(t)$ appear. For $Q_i = 0.6$ and $Q_i = 2.0$, also oscillations in $P(t)$ appear. For $Q_i = 0.2$ and $Q_i = 2.0$, the amplitudes of these oscillations decay, and the oscillations damp out. Hence, after sufficient time a steady state is reached, if $Q_i = 0.2$ or $Q_i = 2.0$. The steady state variables $\omega(r)$, $\overline{S}(r)$ and $\overline{Z}(r)$ are found to be discontinuous at $r = r^*$.
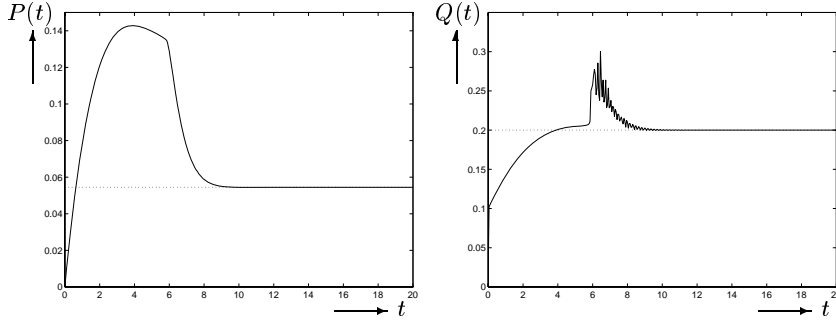

Fig. 7. The pressure $P(t)$ and the volumetric flow rate $Q(t)$ as functions of time t, for $\varepsilon = 0.005$, $\chi = 1$ and $Q_i = 0.2$. The *dotted lines* correspond to the steady state values

For $Q_i = 0.6$, however, we observe in Fig. 8 that the amplitude of the oscillations in $P(t)$ and $Q(t)$ fails to decay and remains constant after a certain instant. Hence, for $Q_i = 0.6$, the functions $P(t)$ and $Q(t)$ do not settle to a stationary value within the time interval of computation, indicating that no steady state is attained. Instead, $P(t)$ and $Q(t)$ show so-called persistent oscillations. To establish for which inlet flow rates Q_i a steady state is attained when $\varepsilon = 0.005$ and $\chi = 1, 2, 6$, we compute the transient flow for several flow rates, varying from $Q_i = 0$ to $Q_i = 3.0$. The outcome of the computations for $\chi = 1$ is that a steady state is reached for $Q_i \leq 0.35$ and for $Q_i \geq 0.90$.
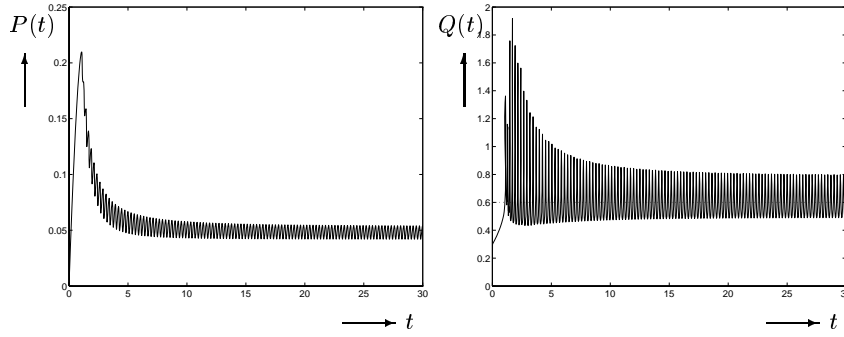
Fig. 8. The pressure $P(t)$ and the volumetric flow rate $Q(t)$ as functions of time t, for $\varepsilon = 0.005$, $\chi = 1$ and $Q_i = 0.6$
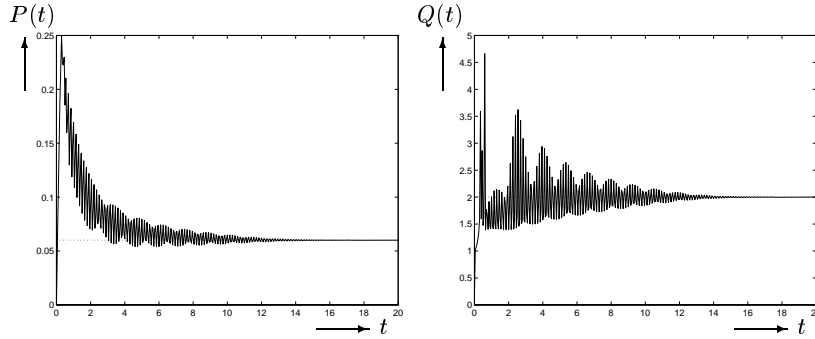

Fig. 9. The pressure $P(t)$ and the volumetric flow rate $Q(t)$ as functions of time t, for $\varepsilon = 0.005$, $\chi = 1$ and $Q_i = 2.0$. The *dotted lines* correspond to the steady state values $\overline{P} = \lim_{t\to\infty} P(t)$ and $\overline{Q} = \lim_{t\to\infty} Q(t)$

This steady state is classical when $Q_i \leq \overline{Q}_{crit} = 0.1678$, and corresponds to spurt flow when $\overline{Q}_{crit} < Q_i \leq 0.35$ or $Q_i \geq 0.90$. For values of Q_i close to 0.35 or 0.90, the time interval within which the flow settles to a steady state, becomes very large. For $0.40 \leq Q_i \leq 0.80$, however, the functions $P(t)$, $Q(t)$, $w(r,t)$, $S(r,t)$ and $Z(r,t)$ show persistent oscillations and fail to settle to stationary values within the time interval of computation. The computations for $\varepsilon = 0.005$ and $\chi = 2$ disclose that the transient flow behaviour is similar to that observed when $\varepsilon = 0.005$ and $\chi = 1$. For $0.40 \leq Q_i \leq 0.65$ persistent oscillations occur, and the flow fails to settle to a steady state. For $\varepsilon = 0.005$ and $\chi = 6$, the numerical computations reveal that a steady state is reached after sufficient time, for each value of the inlet flow rate Q_i considered.

In Fig. 6b. the flow curve of the steady state pressure $\overline{P}$ versus Q_i is plotted for $\varepsilon = 0.005$ and $\chi = 1, 2, 6$. The computed points $(Q_i, \overline{P})$ are marked by a cross ($\times$). The gaps in the flow curves for $\chi = 1$ and $\chi = 2$ correspond to flow rates Q_i for which persistent oscillations occur and no

steady state is attained. We observe that the gap becomes smaller if χ is changed from $\chi = 1$ to the larger value $\chi = 2$, and has disappeared when $\chi = 6$.

Conclusions

We have considered 3-dimensional constitutive models for polymeric fluids. We have found that the stationary shear curve can be nonmonotone, yielding a non-unique solution for the stationary shear rate $\omega(r)$. This nonmonotony is crucial for the existence of

- a sudden increase in the flow rate in pressure-driven extrusion at a certain critical pressure gradient;
- persistent oscillations in pressure and flow rate in piston-driven extrusion.

Both phenomena are typical for the flow instability called spurt. Here, we have maintained the no-slip boundary condition at the wall of the capillary. Accordingly, spurt flow is associated with internal properties of the polymeric melt, and is therefore referred to as a *constitutive instability*.

From the numerical results presented here we infer that a bounded range $\mathcal{R} = (\overline{Q}_m, \overline{Q}_M)$ of inlet flow rates Q_i exists, for which persistent oscillations occur and no steady state is attained. At $Q_i = \overline{Q}_m$ and $Q_i = \overline{Q}_M$, the transition from a steady state to a state of persistent oscillations and vice versa takes place. The size of $\mathcal{R}$ depends on the value of ε as well as on the value of χ: for $\varepsilon = 0.02$ and $\chi = 1, 2, 4$, and for $\varepsilon = 0.005$ and $\chi = 6$, the range $\mathcal{R}$ is empty, whereas for $\varepsilon = 0.005$ and $\chi = 1, 2$, the range $\mathcal{R} = (\overline{Q}_m, \overline{Q}_M)$ is not empty. For $\varepsilon = 0.005$ and $\chi = 1$, the range $\mathcal{R}$ has transition points $\overline{Q}_m$ between 0.35 and 0.40, and $\overline{Q}_M$ between 0.80 and 0.90. For $\varepsilon = 0.005$ and $\chi = 2$, the range $\mathcal{R}$ has transition points $\overline{Q}_m$ between 0.35 and 0.40, and $\overline{Q}_M$ between 0.65 and 0.70. Hence, we conclude that the range $\mathcal{R}$ becomes smaller with increasing χ.

Finally, we mention some further results from the thesis of Aarts, [1],

- Based on the numerical results presented in Fig. 11, the frequency of the persistent oscillations is calculated by means of a Fourier spectral analysis. These frequencies are compared with the frequencies that come up as a solution of a linear stability analysis of the steady state solution. This comparison shows a perfect correspondence between the numerical and the analytical results.
- The influence of the deformation history has been elucidated by numerical simulations of loading and unloading processes. The following peculiarities are observed:
    - the boundary of the spurt layer remains fixed also after unloading (shape memory);
    - persistent oscillations may occur after unloading to supercritical as well as to subcritical flow rates;

> – the deformation history of the melt affects the transient flow behaviour and the steady state attained.

- The models with one relaxation rate and supplied by a Newtonian term as considered here, are compared with models having two, sufficiently widely spaced, relaxation rates. Similar results are obtained for these latter models (Den Adel).

Results in connection with this project

1. Aarts, A.C.T., Analysis of the Flow Instabilities in the Extrusion of Polymeric Melts, Ph.D.Thesis, Eindhoven University of Technology (1997).
2. Aarts, A.C.T., and A.A.F.van de Ven, Transient Behaviour and Stability Points of the Poiseuille Flow of a KBKZ-fluid. J. Eng. Math., 29 (1995), 371-392.
3. Aarts, A.C.T., and A.A.F.van de Ven, Instabilities in the Extrusion of Polymers due to Spurt. In: Progress in Industrial Mathematics at ECMI94, Kaiserslautern; ed. H. Neunzert, Wiley-Teubner, Chichester, 1996, pp. 216-223.
4. Aarts, A.C.T., and A.A.F.van de Ven, The Occurrence of Periodic Distortions in the Extrusion of Polymeric Melts, Continuum Mechanics and Thermodynamics, 11 (1999), 113-139.
5. Adel, R.den, Differences and Equivalences between one Relaxation Rate and a Relaxation Spectrum, Master's Thesis, Eindhoven University of Technology, Eindhoven, August 1996.

2.4   Discrete Melt Fracture Models

The results presented here are mainly from the PhD-thesis of Den Doelder, [2], (performed at EUT):

Design and Implementation of Polymeric Melt Fracture Models.

by: C.F.J.den Doelder.

The main types of melt fracture, showing up as extrudate distortions, can be related to a specific region in the processing geometry:

- surface distortions: initiated near the die exit region,
- spurt distortions: initiated near the die land region,
- volume distortions: initiated near the die entry region.

A simple mathematical model for *spurt* is presented. Spurt is a type of instability occurring in the extrusion of polymer melts. It shows up by periodical jumps in the volumetric flow rate and by relaxation oscillations in the pressure. In capillary flow, spurt is characterized by the occurrence of a thin layer of very high shear rates near the capillary wall (the spurt zone). By splitting up the flow region in a (narrow) spurt zone, where the viscosity is very

small, and a kernel, with $O(1)$-viscosity, a discrete model for spurt flow is constructed. At the wall a no-slip condition is maintained (cf [8]). The model is compared with a model allowing slip, and a complete equivalence is shown (cf [4]). On the basis of the model, spurt or relaxation oscillations are found, which are, qualitatively, in correspondence with experimental observations. When an extrusion process is in the spurt regime, the extrudate shows alternating smooth and distorted regions. In this stage, the volumetric flow rate Q periodically jumps between a lower value ($\Rightarrow$ *smooth surface: classical flow*) and a much higher value ($\Rightarrow$ *distorted surface: spurt flow*). Also the pressure gradient, driving the capillary flow, shows oscillations. These oscillations are many times observed in experiments, and look like relaxation oscillations. Therefore, we shall refer to them as *spurt* or *relaxation oscillations*. In *spurt*, as it is to be understood here, the flow profile looks strongly different in two regions:

- in the inner region (the kernel) the velocity gradient is small and the flow profile is flat, looking very much like cork flow; in this inner region the flow is similar to classical Poiseuille flow;
- in a very small region close to the wall the velocity profile is very steep, yielding very large values for the velocity gradient; this region is called the spurt zone.

The extrusion device we consider consists of a huge barrel filled with polymeric melt, closed at one side by a movable plunger, and on the other side connected to a narrow cylindrical capillary (see Fig. 1). The moving plunger compresses the polymeric melt in the barrel and forces it to flow into the capillary. In the barrel a uniform state is assumed, and the polymeric melt in it is taken to be compressible. The unknowns here are the pressure $P(t)$ and the volumetric flow rate $Q(t)$ flowing from the barrel into the capillary. The relations to be used here are:

- a global balance law for the total mass of the melt in the barrel;
- a constitutive (linearly elastic) compressibility law, relating the pressure to the density.

This results in the following relation, in dimensionless form, (see (1))

$$\frac{dP(t)}{dt} = -(Q(t) - Q_i). \tag{57}$$

For the shear dominated flow in the capillary we assume:

- laminar incompressible flow;
- pressure linear in the axial coordinate z;
- inertia term negligible.

The axial component of the equation of motion then yields the following relation for the, dimensionless, shear stress τ (see (13) and (38); $T_{rz} \to -\tau$)

$$\tau(r,t) = 4rP(t), \qquad 0 \le r < 1. \tag{58}$$

These relations must be supplemented by

- a constitutive equation for the shear stress τ ;
- a relation for the volumetric flow rate (see (45))

$$Q(t) = \int_0^1 r^2 w(r,t) dr. \qquad (59)$$

Two results of the theory for constitutive instabilities motivated us to propose a discrete model consisting of two distinct Newtonian fluids in concentric die regions. These results are

- The non-monotony of the stationary shear curve (total shear stress at the wall versus shear rate), having as a consequence that the apparent viscosity in the spurt zone is much smaller than the one in the kernel.
- The shape memory, implying that the thickness of the spurt layer remains constant during spurt.

Discrete model

Our model is based on the possible existence of a spurt zone in capillary flow. The existence of such a spurt zone is regulated by a switch function. During spurt, the spurt zone reaches from $r = r^* < 1$, to $r = 1$, $(1 - r^* \ll 1)$, whereas in classical flow no spurt zone exists $(r^* = 1)$. The discrete model consists of a set of three equations for the pressure $P(t)$, the volumetric flow rate $Q(t)$ and the thickness of the spurt zone $(1 - r^*(t))$. This set can be solved analytically. The analytical calculations make use of asymptotics that are based on different typical time scales during distinct phases of the process (spurt flow versus classical flow). The obtained analytical results clearly predict relaxation oscillations.

The difference between classical flow and spurt flow is essentially expressed in τ. Both in the classical region as well as in the spurt zone a linear (Newtonian) relation for the shear stress is assumed, however, with different values for the viscosity.

1. In classical flow we take (the normalized viscosity is one, here) $\tau = w$, yielding
$$\tau(r,t) = w(r,t) = 4rP(t). \qquad (60)$$

2. In the spurt zone, due to the very high shear rate, the viscosity is much smaller; so there
$$\tau(r,t) = \varepsilon w(r,t) = 4rP(t), \qquad 0 < \varepsilon \ll 1. \qquad (61)$$

3. Transitions from classical to spurt flow, and vice versa, are very fast.
4. Shape memory causes the thickness of the spurt zone to remain constant during spurt.

Our discrete model is formulated in the following three sets of equations:
A. The spurt zone reaches from $r = r^* \leq 1$ to $r = 1$, where $(1 - r^*) \ll 1$. If $r^* = 1$: no spurt zone exists (classical flow). Hence,

$$w(r,t) = 4rP(t), \quad 0 \leq r < r^* ; \quad w(r,t) = \frac{4rP(t)}{\varepsilon}, \quad r^* < r \leq 1. \qquad (62)$$

B. The volumetric flow rate, (59), can be evaluated into

$$Q(t) = P(t)\left((r^*)^4 + \frac{(1 - (r^*)^4)}{\varepsilon}\right) \approx P(t)\left(1 + \frac{4}{\varepsilon}(1 - r^*)\right), \qquad (63)$$

since $(1 - r^*) \ll 1$.
We define the normalized thickness of the spurt zone by

$$R(t) = (1 - r^*)/\varepsilon, \quad \Rightarrow \quad Q(t) = P(t) + 4R(t)P(t). \qquad (64)$$

C. Finally, we propose an evolution equation for $R(t)$ as

$$\frac{dR}{dt} = -\lambda[R(t) - \alpha H(P - B(Q))], \qquad (65)$$

with λ and α material parameters, H the Heaviside function, and $B(Q)$ a switch curve, as defined in Fig. 10. Since, by assumption, the transition from classical to spurt flow, and vice versa, is very fast, we have $\lambda \gg 1$.
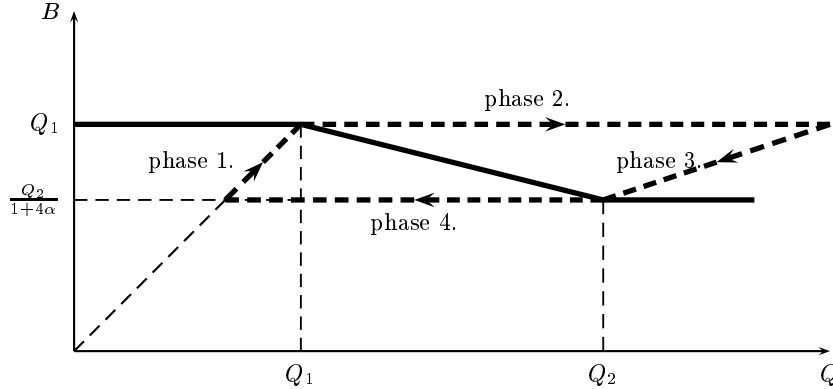

Fig. 10. The switch curve $B(Q)$ (*bold line*). *Dashed line* is relaxation loop

Recapitulating, we have the following discrete model:

- Unknowns: $P(t), \quad Q(t), \quad R(t)$.

- Equations

$$\frac{dP(t)}{dt} = Q_i - Q(t), \tag{66}$$

$$Q(t) = (1 + 4R(t))P(t), \tag{67}$$

$$\frac{dR(t)}{dt} + \lambda R(t) = \alpha \lambda H(P - B(Q)). \tag{68}$$

- Initial conditions: $P(0) = R(0) = 0.$

Comparison spurt and slip model

The results of the theory of constitutive instability are compared to those for a stick-slip model, based on a model for slip at the wall, in agreement with a slip law (cf. [9] or [4]). In this slip model, $v(1, t)$ can be either larger than zero or equal to zero, depending on whether slip occurs or not. When slip starts, the flow rate suddenly increases. The slip velocity at the wall is taken proportional to the maximum shear stress at the wall, which at its turn is proportional to the pressure $P(t)$. The appearance of slip is governed by an evolution equation of the same type as the one for $R(t)$. Thus, in this model, the velocity at the wall is governed by the relation

$$v(1, t) = G(t)P(t), \tag{69}$$

where $G(t)$ satisfies a similar evolution equation as $R(t)$ in (11). Stick or slip occurs accordingly to $G(t) = 0$, or $G(t) > 0$, respectively.
Here, everywhere in the flow $\tau = w = 4rP(t)$, yielding for the flow rate

$$Q(t) = 2 \int_0^1 rv(r, t)dr = v(1, t) + \int_0^1 r^2 w(r, t)dr = (1 + G(t))P(t). \tag{70}$$

Hence, when $G(t) \to 4R(t)$ exactly the same model as (66)–(68) follows.
For both models relaxation oscillations of similar type in both the pressure $P(t)$ and the volumetric flow rate $Q(t)$ are found. Hence, from a mathematical point of view, the two models are equivalent.

Analysis discrete model

The nonlinear system (66)–(68) can be solved analytically if we make use of asymptotics that are based on $\lambda \gg 1$ (fast transitions). For this, we distinguish four phases, of which phase 1. represents classical flow, phase 3. spurt flow (or *slip*), while the phases 2. and 4. are transition phases from classical to spurt flow (*stick to slip*) and vice versa, respectively. Hence, in phase 1., $R(t) = 0$, whereas in phase 3., $R(t) = \alpha$. During the very short $(O(\lambda^{-1}))$ phases 2. and 4., $R(t)$ jumps from $0 \to \alpha$, and from $\alpha \to 0$, respectively.

Since $R(t)$ is constant during the phases 1. and 3. (shape memory), the system (66)–(68) is linear then and can easily be solved. At the other hand, the transition phases are so short $(O(\lambda^{-1}))$ that the changes in $P(t)$ according to (66) are also of $(O(\lambda^{-1}))$ and, hence, negligible in an approximation for $\lambda \gg 1$. Thus, $P(t)$ may be taken constant during these phases, and again the system (66)–(68) is linear then and easy to solve.

Therefore, we distinguish the following four phases:

Phase 1. $\underline{0 < t < t_1}$; classical flow.

In this initial phase $P < B(Q)$ and, hence, $H(P - B(Q)) = 0$. Then (68), with $R(0) = 0$, yields $R(t) = 0$. This reduces (66)–(68) to

$$\frac{dP}{dt} = Q_i - Q(t), \qquad P(0) = 0,$$
$$Q(t) = P(t), \tag{71}$$

the solution of which reads

$$P(t) = Q(t) = Q_i(1 - e^{-t}). \tag{72}$$

The end of phase 1. is at $t = t_1$, where t_1 is the time where $P(t)$ reaches for the first time the switch curve $B(Q)$. Hence (see Fig. 10), $P(t_1) = Q_1$, yielding

$$t_1 = \ln(\frac{Q_i}{Q_i - Q_1}), \tag{73}$$

provided $Q_i > Q_1$.

We note that $t_1 = O(1)$, which justifies our time scaling.

Phase 2. $\underline{t_1 < t < t_2}$: transition from classical to spurt flow.

Since $P(t)$ crosses $B(Q)$ from below at $t = t_1$, we assume that during this phase $P > B(Q)$, so $H(P - B(Q)) = 1$.

For this phase we introduce a new time scale: $\tau = \lambda(t - t_1)$, such that (66)–(68) becomes $(R = R(\tau)$, etc.)

$$\frac{dR}{d\tau} + R(\tau) = \alpha, \qquad R(0) = 0,$$
$$\frac{dP}{d\tau} = \frac{1}{\lambda}(Q_i - Q(\tau))(= O(\lambda^{-1})), \quad P(0) = Q_1,$$
$$Q(\tau) = (1 + 4R(\tau))P(\tau). \tag{74}$$

The solution of this system reads

$$P(\tau) = P(0)(1 + O(\lambda^{-1})) \approx Q_1,$$
$$R(\tau) = \alpha(1 - e^{-\tau}) \ (\to \alpha),$$
$$Q(\tau) = [1 + 4\alpha(1 - e^{-\tau})]Q_1 \ (\to (1 + 4\alpha)Q_1). \tag{75}$$

We define the end of phase 2. as $\tau = \tau_2$, such that $e^{-\tau_2} = \lambda^{-1}$. This yields

$$\tau_2 = \ln\lambda, \quad \text{or} \quad t_2 = t_1 + \frac{\ln\lambda}{\lambda} = t_1(1 + O(\lambda^{-1})). \tag{76}$$

So, indeed $\tau_2 = O(1)$, implying that the time that phase 2. lasts is very short $(O(\lambda^{-1}))$ compared to phase 1.

Phase 3. $\underline{t_2 < t < t_3}$; spurt flow.

In this phase we assume $P > B(Q)$ (see Fig. 10), so $H(P - B(Q)) = 1$. Since $(75)^3$ yields $R(t_2) = \alpha(1 + O(\lambda^{-1})) \approx \alpha$, for $\lambda^{-1} \to 0$, (68) renders $R(t) = \alpha$, for all $t \in (t_2, t_3)$.
With the new time scale $\tau = (t - t_2)$, (66)–(68) reduces to $(P = P(\tau)$, etc.)

$$\frac{dP}{d\tau} = Q_i - Q(\tau), \quad P(0) = Q_1,$$
$$Q(\tau) = (1 + 4\alpha)P(\tau). \tag{77}$$

The solution of this system reads

$$P(\tau) = \frac{Q(\tau)}{1 + 4\alpha} = \frac{Q_i}{1 + 4\alpha} + \left[Q_1 - \frac{Q_i}{1 + 4\alpha}\right]e^{-(1+4\alpha)\tau}. \tag{78}$$

Since phase 3. always runs along the line $P = Q/(1 + 4\alpha)$ in a $P - Q$-diagram, it must be so that if this line crosses the switch curve $B(Q)$ this happens in the point $P = B(Q_2) = Q_2/(1 + 4\alpha)$. According to (78), $Q(\tau) \to Q_i$, for $\tau \to \infty$. As $Q \to Q_i$, there are now two possibilities:

1. If $Q_i > Q_2$,
   then $P(\tau) \to Q_i/(1 + 4\alpha) > B(Q_i) = Q_2/(1 + 4\alpha)$
   In this case no transition takes place, and phase 3. tends to a final stationary spurt state, in which $(P(\tau), Q(\tau)) \to (Q_i/(1 + 4\alpha), Q_i))$, for $\tau \to \infty$.
2. If $Q_i < Q_2(< (1 + 4\alpha)Q_1$,
   then a transition to classical flow takes place when $Q(t)$ reaches $Q_2 > Q_i$, and then phase 4. starts at $t = t_3(< \infty)$. Here, t_3 is such that $Q(t_3) = Q_2$, yielding
   $$t_3 = t_2 + \frac{1}{(1 + 4\alpha)}\ln\left(\frac{(1 + 4\alpha)Q_1 - Q_i}{Q_2 - Q_i}\right) . \tag{79}$$

We assume case 2. to hold, and we proceed with phase 4. We shall see that in this case relaxation oscillations occur.

Phase 4. $\underline{t_3 < t < t_4}$; transition from spurt to classical flow.

At $t = t_3$, $P(t)$ crosses the switch curve coming from above, so during this phase we assume $P < B(Q)$, and thus $H(P - B(Q)) = 0$

With the new time scale $\tau = \lambda(t - t_3)$, (66)–(68) reduces to ($R = R(\tau)$, etc.)

$$\frac{dR}{d\tau} + R(\tau) = 0, \qquad R(0) = \alpha,$$

$$\frac{dP}{d\tau} = \frac{1}{\lambda}(Q_i - Q(\tau))(= O(\lambda^{-1})), \quad P(0) = Q_2/(1 + 4\alpha),$$

$$Q(\tau) = (1 + 4R(\tau))P(\tau). \tag{80}$$

The solution of this system reads

$$P(\tau) = \frac{Q_2}{(1 + 4\alpha)}(1 + O(\lambda^{-1})),$$

$$R(\tau) = \alpha e^{-\tau} \quad (\to 0),$$

$$Q(\tau) = \frac{Q_2}{(1 + 4\alpha)}(1 + 4\alpha e^{-\tau}). \tag{81}$$

Analogous to phase 2., phase 4. ends at $t = t_4 = t_3(1 + O(\lambda^{-1}))$.
At $t = t_4$, phase 1. starts anew, but now not from $P(0) = Q(0) = 0$, but from

$$P = Q = Q_2/(1 + 4\alpha).$$

This brings us to:

Phase 5. $\underline{t_4 < t < t_5}$; classical flow.

Analogous to Phase 1., the solution now reads

$$P(t) = Q(t) = Q_i + \left(\frac{Q_2}{1 + 4\alpha} - Q_i\right)e^{-(t - t_4)}. \tag{82}$$

This phase ends at $t = t_5$ when $Q(t_5) = Q_1$, yielding

$$t_5 = t_4 + \ln\left(\frac{Q_i - Q_2/(1 + 4\alpha)}{Q_i - Q_1}\right), \tag{83}$$

after which a phase identical to phase 2. follows.

Thus, a loop is followed as depicted by the dashed line in Fig. 10. Since this dashed line is a closed loop, it represents a periodic phenomenon. Its behaviour is of relaxation type, because the phases 2. and 4. are extremely short. Therefore, we call this a relaxation oscillation. The period of one oscillation is $(t_3 - t_2) + (t_5 - t_4)$, or

$$T_{os} = \ln\frac{((1 + 4\alpha)Q_1 - Q_i)((1 + 4\alpha)Q_i - Q_2)}{(1 + 4\alpha)(Q_2 - Q_i)(Q_i - Q_1)}, \tag{84}$$

for $\lambda^{-1} \approx 0$. The behaviour of the pressure $P(t)$ and the volumetric flow rate $Q(t)$ during these relaxation oscillations is depicted in Fig. 11.
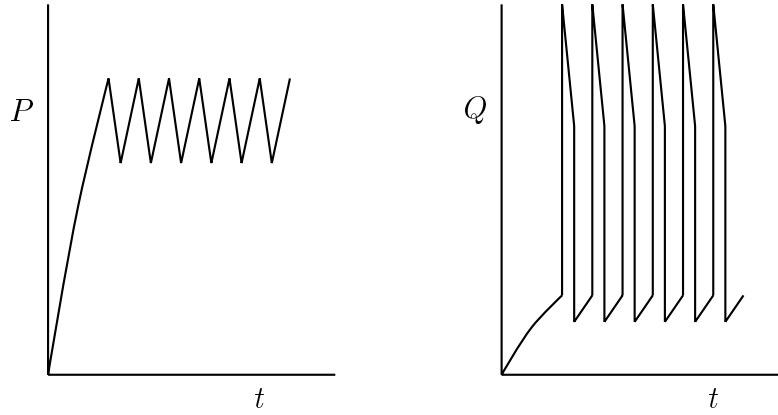
Fig. 11. Relaxation oscillations for the pressure $P(t)$ and the volumetric flow rate $Q(t)$ ($Q_1 = 1$, $Q_2 = 3$, $Q_i = 2$, $\alpha = 1$, and $\lambda = 1000$)
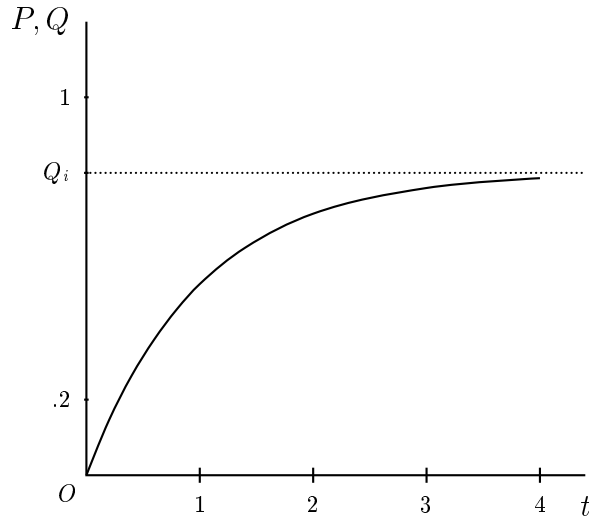

Fig. 12. The pressure $P(t)$ and the flow rate $Q(t)$ as function of time t for $Q_i = 0.8 < Q_1$ (classical flow)

Results

Our model described by the system (66)–(68) is characterized by the parameter set $\{Q_1, Q_2, \alpha, \lambda\}$ plus the prescribed inlet flow rate Q_i. In the preceding section we have seen that dependent on the value of Q_i different

types of capillary flow can occur. We distinguish three regimes for Q_i, knowing $Q_i < Q_1$, $Q_1 < Q_2 < Q_1$, and $Q_i > Q_2$. For the numerical results in this section, the following fixed values for the parameters are used:

$$Q_1 = 1 \,, Q_2 = 3 \,, \alpha = 1 \,, \lambda = 1000 \,.$$

We find:

- In the first regime, $Q_i < Q_1$, the flow is classical, just like a Poiseuille flow. Since there is no spurt zone, the velocity profile is smooth. The pressure and the flow rate tend monotone to their stationary values, according to (72). This behaviour is depicted in Fig. 12.
- In the second regime $Q_1 < Q_i < Q_2$, persistent relaxation oscillations occur. The flow periodically jumps from classical to spurt and vice versa, and large jumps in the pressure and, especially, the flow rate are found. The value of the flow rate is relatively high during spurt, and low during classical flow. Typical relaxation oscillations in $P(t)$ and $Q(t)$ in case $Q_i = 2$ are depicted in Fig. 11.
- In the third regime $Q_i > Q_2$, the flow again tends to a stationary state, but now to one in which spurt occurs. The spurt zone is fixed to $R = \alpha$, and pressure and flow reach the stationary values $\bar{P} = Q_i/(1 + 4\alpha)$, and $\bar{Q} = Q_i$, respectively, according to (78). In this regime we can further distinguish between $Q_i < (1 + 4\alpha)$ and $Q_i > (1 + 4\alpha)$. In case $Q_i < (1 + 4\alpha)$, an overshoot in both $P(t)$ and $Q(t)$ occurs, before they reach their final state. This overshoot at $t = t_1$ is depicted in Fig.13, for the case that $Q_i = 4$. If $Q_i > (1 + 4\alpha)$, no overshoot occurs; in this case the steady state is reached in a monotone way.

A finite range of prescribed inlet flow rates Q_i can be found for which relaxation oscillations can occur. This is illustrated by the simulation of a realistic loading process, depicted in Fig. 14, in which only for a restricted range of Q_i−values spurt oscillations show up. For Q_i−values below this range ($Q_i < Q_1$) the flow tends to a stationary classical (Poiseuille) flow, whereas for values beyond this range ($Q_i > Q_2$) the flow tends to a stationary spurt flow (having a fixed spurt layer).

Improvement of the Model

A lot of experimental data on especially extrusion instabilities are known (in literature and from internal experiments at DOW). Comparison of our analytical results as depicted in Figs. 11 −14 with experimental results indicates a good *qualitative* agreement. However, for a *quantitative* agreement, some further modifications of the model presented here are needed. This is done by Den Doelder in his PhD-thesis (see also [10]). These modifications concern:

- A nonlinear evolution equation, emanating from a nonlinear slip law. This nonlinear slip law relates the slip velocity to the *square* of the wall shear
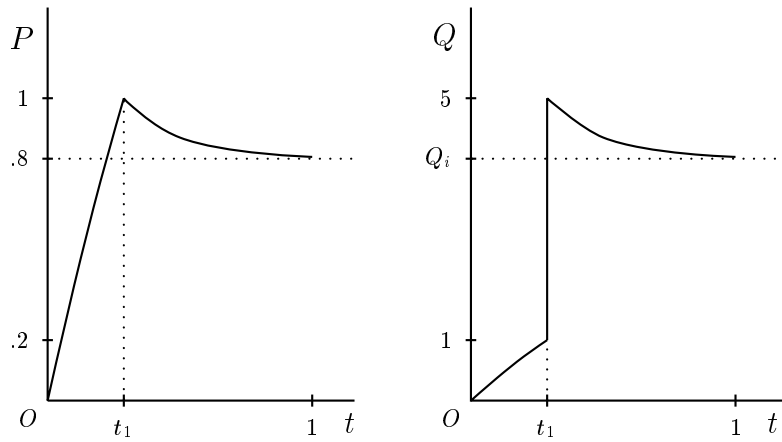
Fig. 13. The pressure $P(t)$ and the flow rate $Q(t)$ as function of time t for $Q_i = 4 > Q_2$ (spurt flow)

Fig. 14. The pressure $P(t)$ as function of time t for a loading process in which Q_i is stepwise increased at time steps T, with $T = 2.1$, according to the sequence $\{0.4,\ 0.8,\ 1.2,\ 1.8,\ 2.4,\ 3.6,\ 4.8\}$

stress. Translated to our model, this would imply that relation (67) must become nonlinear in so far that $P(t)$ must be replaced by $P^2(t)$.

- An improved constitutive model for the polymer fluid. The Newtonian model is replaced by a power law (shear thinning) model (generalised Newtonian ; no elasticity).
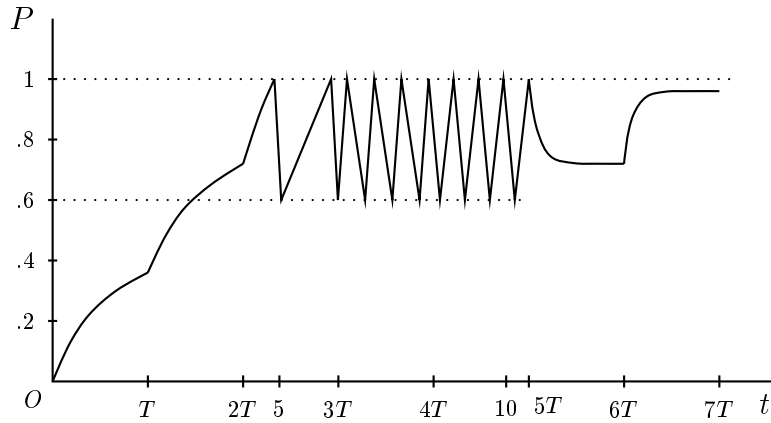- Elastic effects in the die exit and entry region are incorporated in a pressure correction term (Bagley correction).
- The time dependence of the length l of the barrel ($l = l(t) = l(0) - V_0 t$) is taken into account.

The numerical results of this improved model are compared with experimental data from experiments performed at DOW. The calculated relaxation oscillations of the pressure are in very good *quantitative* correspondence with these data. The absolute pressure values, the amplitudes of the oscillations and the period of the oscillations compare very well with the experimental values (cf. [10]).

Conclusions

We state the following conclusions:

- The discrete models, either with no-slip and spurt zone or with a stick-slip law, explain relaxation oscillations in $P(t)$ and $Q(t)$.
- Comparison with experimental results indicates a good qualitative and quantitative agreement with experimentally observed relaxation oscillations in $P(t)$.

Results in connection with this project

1. Molenaar, J. and R.J. Koopmans, Modeling Polymer Melt-flow Instabilities, Journal of Rheology, 38 (1994), 99-109.
2. Doelder, C.F.J. den, Sharkskin and Spurt in JSO Modelled Polymer Extrusion, Eindhoven University of Technology, Final report of the postgraduate programme Mathematics for Industry, ISBN 90 5282 727 3 (1996), Eindhoven.
3. Doelder, C.F.J. den, Design and Implementation of Polymeric Melt Fracture Models. Ph.D.Thesis, Eindhoven University of Technology (1999).
4. Doelder, C.F.J. den, R.J. Koopmans, J. Molenaar and A.A.F. van de Ven, Comparison of Wall Slip and Constitutive Instability Spurt Models, Journal of Non-Newtonian Fluid Mechanics, 75 (1998), 25-41.
5. Doelder, C.F.J. den, R.J. Koopmans and J. Molenaar, Quantitative Modelling of HDPE Spurt Experiments Using Wall Slip and Generalised Newtonian Flow, Journal of Non-Newtonian Fluid Mechanics, 79 (1998), 503-514.
6. Ven, A.A.F. van de, Comparing Stick and Slip Models for Spurt in the Extrusion of Polymeric Melts. In: Progress in Industrial Mathematics at ECMI98, eds: L. Ackeryd, J. Bergh, P. Brenner, R. Petterson (Proceedings of 10th ECMI-Conference, ECMI 98, Göteborg.) pp. 154-162. Teubner, Stuttgart, 1999.

7. Ven, A.A.F. van de, Spurt in the Extrusion of Polymeric Melts; Discrete Models for Relaxation Oscillations. In: Complex Flows in Industrial Processes; ed. A. Fasano, 2000.

3 Injection Moulding

3.1 Introduction

The filling phase of an injection moulding process in a straight cavity, consisting of the narrow space between two adjacent parallel circular plates, inclusive the front motion at the free boundary of the flow, should be analysed. The cavity is *thin*, meaning that the distance between the plates is much smaller than their radius. The injection inlet is at the center of the plate and the resulting flow is rotationally symmetric. For some applications, the flow will be considered as being two-dimensional. Besides the flow fields (velocity, stresses) also the temperature and pressure fields must be calculated. Thermal effects are due to cooling at the walls and to viscous dissipation; pressure effects are due to compressibility and to interactions with thermal fields. The material coefficients of the melt (especially the viscosity) are strongly temperature and/or pressure dependent. The melt can be modelled as either a generalised Newtonian fluid or, if necessary, as a nonlinear viscoelastic fluid. In any case, the viscosity should be dependent on both shear rate (*shear thinning*) as well as temperature.

The possibility of thermally induced instabilities of the front flow will be studied. An asymmetric flow front causes differences in temperature, and thus also in viscosity, due to different thermal contacts at upper and lower wall of the cavity. These differences in viscosities can induce an ongoing asymmetry of the flow front, which can result into instability.

One specific application of injection moulding is in the production of compact discs (CD's). For an adequate description of this process, a thermoviscoelastic model is needed. Essential in this modelling is a simulation of the cooling of the hot polymer melt in the mould or cavity. Another point of utmost practical importance is the calculation of residual stresses and deformations in the final product.

The latter two points mentioned above are the subject of two PhD-projects to be performed at EUT in co-operation with industry. These projects are

1. H.J.J. Gramberg:
   Front Instabilities in Injection Moulding.
2. S.M.P. Smolders:
   A Thermoviscoelastic Model for Injection Moulding.

However, since the second project started only very recently, and as this is mainly confidential research, we shall discuss here only the first project. Because also this project is still in an initial state, we shall present only the results obtained up to now, together with prospects for further research.

3.2   Problem Description

The cylindrical cavity we consider here has height $2h$ and radius R, where $h \ll R$. The rotationally symmetric flow in the cavity is described in cylindrical coordinates (r, z). In the *filling phase* when the fluid is entering the cavity, the flow has a front which is an unknown free surface. The fluid occupies the flow region Ω behind the front (see Fig. 15). Let $r = R_f(z, t)$ denote the radial position of a point on the flow front on height z. Then the flow region is given by

$$\Omega(t) = \{(r, z) \mid R_n < R_i < r < R_f(z, t) < R, \ -h < z < h \} . \tag{85}$$
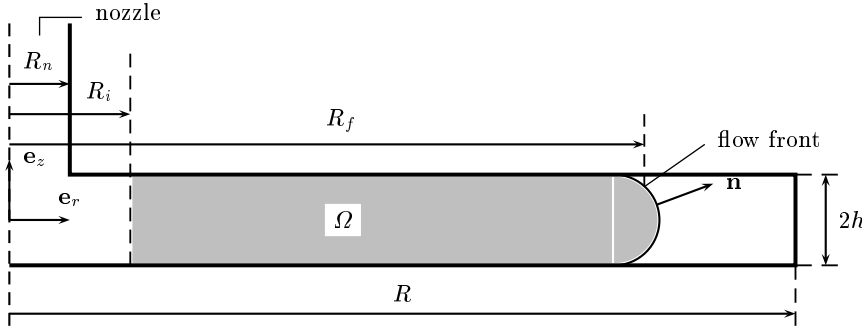

Fig. 15. The flow region G in the cavity.

To model the viscoelastic flow in the filling phase (see also [11]), we start with

Local balance equations. The fundamental unknowns in the injection process to be considered here are the velocity $\mathbf{v}(r, z, t) = v_r \mathbf{e}_r + v_z \mathbf{e}_z$, the pressure $p(r, z, t)$ and the temperature $T(r, z, t)$. They are governed by the balance laws of continuum mechanics, here written as

- *Equation of continuity*
$$\dot{\rho} + \rho \nabla \cdot \mathbf{v} = 0 , \tag{86}$$

  where ρ is the density, and $\dot{\rho}$ is its material derivative.
- *Equation of motion*
$$\rho \mathbf{v} = \nabla \cdot \mathcal{T} , \tag{87}$$

  in the absence of body forces, where $\mathcal{T} = \mathcal{T}(r, z, t)$ is the total stress tensor.

- *Balance of energy*

$$\rho \dot{u} = \mathcal{T} : \mathcal{D} - \nabla \cdot \mathbf{q} \, , \tag{88}$$

where u is the internal energy density, $\mathcal{D}$ the rate-of-deformation tensor (see (8)), $\mathbf{q}$ the heat flux vector, while the heat source is assumed zero.

Constitutive equations. The balance equations should be supplemented by constitutive equations for the stresses and the heat flux together with an explicit expression for the internal energy density and, finally, especially for compressible melts a constitutive equation for ρ as function of T and p:

- *Stresses.*
  The total stress tensor is decomposed into a pressure part and an extra stress according to

$$\mathcal{T} = -p\mathcal{I} + \mathcal{S} \, . \tag{89}$$

The extra stress will be described by either a generalised Newtonian model or by a nonlinear viscoelastic model (e.g. Leonov model):
  - For the generalised Newtonian model we have

$$\mathcal{S} = 2\eta \mathcal{D}^d \, , \tag{90}$$

where $\mathcal{D}^d$ is the deviatoric part of $\mathcal{D}$, i.e.

$$\mathcal{D}^d = \mathcal{D} - \frac{1}{3} tr(\mathcal{D})\mathcal{I} \, , \tag{91}$$

and where the viscosity η is a function of the shear rate $\dot{\gamma}$ defined by

$$\dot{\gamma} = \sqrt{2\mathcal{D}^d : \mathcal{D}^d} \, , \tag{92}$$

and the temperature ($\eta = \eta(\dot{\gamma}, T)$).
  - For the Leonov model we have

$$\mathcal{S} = 2\eta_r \mathcal{D}^d + \sum_{k=1}^{K} \tau_k \, , \tag{93}$$

where η_r is the so called retardation viscosity and τ_k are the sub-stresses, having K modes.
- *Heat flux.*
  We use Fourier's law

$$\mathbf{q} = -\lambda \nabla T \, , \tag{94}$$

where the heat conduction coefficient λ still can depend on temperature and pressure.

- *Internal energy density.*
  Using some relations from thermodynamics (a.o. *Gibbs law*), we can derive

  $$\dot{u} = c_p \dot{T} - \frac{\alpha T}{\rho} \dot{p} + \frac{p}{\rho^2} \dot{\rho} , \tag{95}$$

  where α is the coefficient of thermal expansion ($\rho\alpha = \partial\rho/\partial T$) and c_p is the heat capacity at constant pressure ($c_p = \partial u(T, p)/\partial T$).

- *Density*
  Considering for a compressible melt $\rho = \rho(T, p)$, we find

  $$\dot{\rho} = \rho\kappa\dot{p} - \rho\alpha\dot{T} , \tag{96}$$

  where κ is the isothermal compressibility ($\rho\kappa = \partial\rho/\partial p$).
  In case of an incompressible medium, we have $\rho = \rho_0$, and then the pressure $p = p(x, z, t)$ is an unknown field variable; as an extra equation, we then have the incompressibility condition div $\mathbf{v} = \nabla \cdot \mathbf{v} = 0$.

All the material coefficients appearing in the above relations are in general functions of temperature, pressure and shear rate.

Final equations. Substituting the constitutive equations listed above into the local balance equations, we arrive at the following set of equations for the fundamental unknowns p, $\mathbf{v}$ and T:

$$\rho\kappa\dot{p} - \rho\alpha\dot{T} + \rho\nabla \cdot \mathbf{v} = 0 , \tag{97}$$

$$\rho\dot{\mathbf{v}} + \nabla p = \nabla \cdot \mathcal{S} , \tag{98}$$

$$\rho c_p \dot{T} - \alpha T \dot{p} = \mathcal{S} : \mathcal{D} + \nabla \cdot (\lambda \nabla T) . \tag{99}$$

Boundary conditions. We proceed with the boundary conditions on $\partial\Omega$. The boundary $\partial\Omega$ of Ω consists of the following three segments:

1. *Inlet:* $r = R_i > R_n$; $-h < z < h$.
   Here, R_i is chosen a few times h larger than R_n (see Fig. 15), in order to get rid of inlet disturbances. At $r = R_i$ the flow is assumed fully developed and the pressure and the temperature are taken equal to their inlet values. This leads to the boundary conditions (p_i, $V(z)$ and T_i prescribed)

   $$p(R_i, z, t) = p_i ,$$
   $$\mathbf{v}(R_i, z, t) = V(z)\mathbf{e}_z ,$$
   $$T(R_i, z, t) = T_i . \tag{100}$$

2. *Walls of the cavity:* $z = \pm h$; $R_i < r < R_f(\pm h, t)$.
   At these walls no-slip is assumed and the walls are cooled at a prescribed

temperature T_w, which, in general, can still be a function of r and different at the upper and lower wall ($T_w^{\pm}(r)$ prescribed)

$$\mathbf{v}(r, \pm h, t) = \mathbf{0} \ ,$$
$$T(r, \pm h, t) = T_w^{\pm}(r) \ . \tag{101}$$

3. *Flow front*: $r = R_f(z, t) \ ; \quad -h < z < h \ .$

   The flow front is a free boundary, which is assumed free of stress (the pressure in the environment is scaled to zero) and thermally insulated. Moreover, the front moves with a velocity V_f in $z-$direction. This leads to:

$$\mathcal{T}\mathbf{n} = \mathbf{0} \ ,$$
$$((\mathbf{v} - V_f\mathbf{e}_z), \mathbf{n}) = 0 \ ,$$
$$\frac{\partial T}{\partial n} = 0 \ , \qquad \text{at } r = R_f(z, t) \ . \tag{102}$$

The equations and boundary conditions presented above form a complete and consistent system for the simulation of an injection moulding process in a cylindrical cavity between two parallel plates. However, before analysing this system, the equations must be made dimensionless and normalized. This will be done for a specific application in the next section.

3.3   Front Instabilities in Injection Moulding

Aim. General approach

The ultimate aim of this project is to find by analytical means an explanation for the flow front instability, observed in injection moulding. This instability can be either due to thermal effects or to elasticity effects, or to combinations of both. We focus here purely on thermal effects. In order to be able to find analytical solutions, we have to make the model as simple as possible, though keeping the essential features. In our view, the most important feature is the coupling between the viscosity and the temperature of the fluid, as the latter is strongly influenced by the cooling at the walls of the cavity. To explain our view, let us assume there is initially an asymmetric flow front (for instance due to the asymmetric inlet of the mould, which is filled from above) and that at certain time t the contact point of the flow front with the upper wall is farther (in the r-direction) than the corresponding point at the lower wall (i.e. $R_f(+h, t) > R_f(-h, t)$). In that case, the fluid near the upper wall will cool more than the fluid below, and so the fluid will be stiffer (higher viscosity) at the upper wall than at the lower one. Consequently, the fluid will be retarded at the upper wall with respect to the fluid at the lower wall and, thus, the asymmetry will flip. This means that at a somewhat later time the flow front is farther at $z = -h$ than at $z = +h$. This cyclus will repeat

itself and then the front is wobbling. We adhere to this phenomenon the *front instability* we are looking for.

To model the problem described above, we make the following simplifications:

- We assume the fluid to be incompressible ($\alpha = \kappa = \nabla \cdot \mathbf{v} = 0$) and Newtonian, however with a temperature dependent viscosity, i.e.

$$\mathcal{S} = 2\eta(T)\mathcal{D} \ , \qquad \eta(T) = \eta_0 \ e^{-cT} \ , \tag{103}$$

  with c a positive constant.
- We assume all material coefficients occurring in (97), (98) and (99) to be constant.
- We neglect the inertia term in the equation of motion with respect to the viscous term (quasi-static approximation).
- We neglect the viscous dissipation term in the energy equation.
- We consider the cavity to be a two-dimensional slit (this means that we have to replace $\mathbf{e}_r$ and r by $\mathbf{e}_x$ and x, respectively).
- We take the prescribed temperature at the upper and lower wall equal and uniform.
- We assume that the changes in temperature remain small (we are only aiming at the first order effect).

Based on the latter assumption, we split up our problem in a basic problem in which the velocity field and the temperature are uncoupled, plus a perturbation problem in which these fields become coupled in first order.

This results in two separate basic problems:

1. *The velocity problem*, unknowns $\mathbf{v} = \mathbf{v}(x, z, t) = u\mathbf{e}_x + w\mathbf{e}_z$, and $p = p(x, z, t)$, (the temperature is here taken equal to the uniform reference temperature) governed by

$$\nabla \cdot \mathbf{v} = \frac{\partial u}{\partial x} + \frac{\partial w}{\partial z} = 0 \ ,$$

$$-\frac{\partial p}{\partial x} + \eta_0 \triangle u = 0 \ ,$$

$$-\frac{\partial p}{\partial z} + \eta_0 \triangle w = 0 \ , \tag{104}$$

for $(x, z) \in \Omega, \ t > 0$, together with the boundary conditions (here, $x = 0$ corresponds to $r = R_i$)

$$u(0, z, t) = V(z) = \frac{3}{2} \left(1 - \left(\frac{z}{h} \right)^2 \right) \ ,$$

$$u(x, \pm h, t) = 0 \ ,$$

$$\mathcal{S}\mathbf{n} = p \ \mathbf{n} \ , \quad ((\mathbf{v} - V_f\mathbf{e}_z) \cdot \mathbf{n}) = 0 \ , \quad \text{at the front .} \tag{105}$$

From this problem not only the velocity and the pressure can be solved, but also a zeroth order version for the shape of the flow front, yielding a symmetric flow front.

2. *The temperature problem*, unknown $T(x, z, t)$ ($\mathbf{v}$ is known from 1.), with governing equation

$$\frac{\partial T}{\partial t} + (\mathbf{v} \cdot \nabla T) = \kappa \triangle T \ , \tag{106}$$

where $\kappa = \lambda / \rho c_p$: the thermal diffusion constant.
The boundary conditions are

$$T(0, z, t) = T_i \ ,$$
$$T(x, \pm h, t) = T_w \ ,$$
$$\frac{\partial T}{\partial n} = 0 \ , \quad \text{at the front} \ . \tag{107}$$

From this problem the basic temperature distribution can be solved.

To obtain the perturbed problem, we must substitute the perturbed fields, i.e.

$$\mathbf{v} \to \mathbf{v} + \delta \mathbf{v} \ , \quad p \to p + \delta p \ , \quad T \to T + \delta T \ ,$$

into the original equations (97)–(99) and linearise the thus obtained set with respect to the perturbations. Moreover, we must also introduce the perturbed flow front, assumed in an asymmetric shape, and linearise the free-boundary conditions at the front.

Zeroed order velocity problem

As shown by Van Vroonhoven and Kuijpers, [12], the velocity problem formulated in (104) and (105) can be solved by use of complex function theory. For this the velocity and the pressure are expressed in holomorphic functions of a complex variable ($z = x + iz$). By a conformal mapping $z = m(\zeta)$, the flow region Ω is mapped onto the unit circle in the ζ-plane. The problem in the ζ-plane is then reformulated as a Hilbert problem, which is solved analytically. The, still unknown, mapping function $m(\zeta)$ is determined by the free-boundary conditions at the flow front. This function is then approximated by a polynomial of degree N,

$$m(\zeta) \approx m_N(\zeta) = \sum_{k=0}^{N} \mu_k \zeta^k \ . \tag{108}$$

It turns out that already for small values of N (i.e. $N = 2$ or 3) this polynomial renders a very good approximation of the mapping function in the vicinity of the free boundary (i.e. in the right half of the unit circle). With $m(\zeta)$, also the shape of the flow front is determined. From the expressions for the velocity, the flow lines can be calculated.

A reasonable assumption for $m(\zeta)$ turns out to be $m(\zeta) = \zeta$, yielding a purely semi-circular flow front. Especially near the flow front this gives good results for the velocity directly behind that flow front. These results are needed in the next section.

Zeroed order temperature problem

In this section we present a solution of the temperature problem (106) and (107). This solution is quite different in different regions in Ω (e.g. far behind the flow front; near the walls; near the flow front). We first make the equations dimensionless by introducing the dimensionless variables $\hat{t}, \hat{x}, \hat{z}, \hat{\mathbf{v}}$ and $\hat{T}$ by

$$t = \frac{L}{V_f}\hat{t} , \quad x = L\hat{x} , \quad z = h\hat{z} , \quad \mathbf{v} = V_f\hat{\mathbf{v}} , \quad \text{and} \quad \hat{T} = \frac{T - T_w}{T_i - T_w} , \quad (109)$$

where L is a characteristic measure of length in the x-direction, to be specified further on. The specific choice for L depends on which region in Ω we are considering.

In these new variables (106) becomes

$$\frac{\partial \hat{T}}{\partial \hat{t}} + \hat{u}\frac{\partial \hat{T}}{\partial \hat{x}} + \hat{w}\frac{\partial \hat{T}}{\partial \hat{z}} = \hat{\kappa}\left[\frac{\partial^2 \hat{T}}{\partial \hat{z}^2} + \left(\frac{h}{L}\right)^2 \frac{\partial^2 \hat{T}}{\partial \hat{x}^2}\right] , \quad (110)$$

with

$$\hat{\kappa} = \frac{\kappa L}{V_f h^2} , \quad (111)$$

while the boundary conditions (107) become

$$\hat{T}(0, \hat{z}, \hat{t}) = 1 ,$$
$$\hat{T}(\hat{x}, \pm 1, \hat{t}) = 0 ,$$
$$\frac{\partial \hat{T}}{\partial n} = 0 , \quad \text{at the front} . \quad (112)$$

We consider first the:

Region far behind the flow front

$$\underline{(x, z) \in \Omega_0}, \quad \text{where} \quad \Omega_0 = \{(x, z) \mid 0 < x < x_f - kh, \; -h < z < h\},$$

with kh a few times h, and $x_f = V_f t = R_f(h, t) - R_n$ (see Fig. 16).
Here, we choose $L = R$, where $R \gg h$. Moreover, we assume the temperature to be stationary $(T = T(x, z))$ and the flow fully developed. The latter means that

$$\hat{u} = \frac{3}{2}(1 - \hat{z}^2) , \quad \hat{w} = 0 . \quad (113)$$

The factor $3/2$ in (113) is due to the normalisation, which is such that the dimensionless flow rate pertinent to $\hat{u}$ should be 2 (note that the dimensionful

flow rate Q equals $2hV_f$).

Finally, we use the fact that $h \ll L = R$, implying that the diffusion in x-direction can be neglected in the heat equation (110). All this leads to the thin-layer approximation for the heat diffusion equation, i.e. (omitting the hats; the factor $3/2$ is incorporated in κ, i.e $\kappa \rightarrow 2\hat{\kappa}/3$)

$$(1 - z^2)\frac{\partial T}{\partial x} = \kappa\frac{\partial^2 T}{\partial z^2} \ ,$$
$$T(0, z) = 1 \ ,$$
$$T(x, \pm1) = 0 \ , \quad \text{at the front} \ . \tag{114}$$

In practice, the dimensionless diffusion constant κ ($\equiv \hat{\kappa}$) shows up to be rather small ($\kappa = O(10^{-2})$). Therefore, we use asymptotics based on $\kappa \ll 1$. For the *inner solution* (i.e. z not too close to ±1) we then get

$$\frac{\partial T}{\partial x} = 0 \ , \quad \text{and} \quad T(0, z) = 1 \ , \tag{115}$$

yielding

$$T(x, z) = 1 \ , \tag{116}$$

(in fact, of course, $T(x, z) = 1 + O(\kappa)$). Since this solution does not satisfy the boundary conditions at $z = \pm1$, we expect that there is a boundary layer in the vicinity of $z = \pm1$. Since the problem is symmetric with respect to z, we only have to consider the boundary layer near $z = 1$.

For the *outer solution*, holding for z in a *boundary layer* at $z = 1$ (or $z = -1$), where the gradient $\partial T/\partial z$ becomes large, we replace z by

$$z = 1 - \varepsilon\zeta \quad \Longrightarrow \quad \zeta = \frac{1 - z}{\varepsilon} \ , \tag{117}$$

where the small parameter ε ($0 < \varepsilon \ll 1$), representing the thickness of the boundary layer, needs still to be determined.

Substitution of (117) into (114) yields

$$\varepsilon\zeta(2 - \varepsilon\zeta)\frac{\partial T}{\partial x} = \frac{\kappa}{\varepsilon^2}\frac{\partial^2 T}{\partial \zeta^2} \ . \tag{118}$$

Since we want the left-hand side of (118) to be of the same order as the right-hand side, ε must satisfy the following equation

$$\varepsilon^3 = \kappa \quad \Longrightarrow \quad \varepsilon = \sqrt[3]{\kappa} \ . \tag{119}$$

With this choice for ε, (118) can be rewritten as follows

$$2\zeta\frac{\partial T}{\partial x} - \frac{\partial^2 T}{\partial \zeta^2} = \varepsilon\zeta^2\frac{\partial T}{\partial x} \approx 0. \tag{120}$$

The boundary conditions are given by

$$T(0, \zeta) = 1,$$
$$T(x, 0) = 0,$$
$$T(\zeta \to \infty) = 1. \tag{121}$$

We try as a solution of (120) and (121)

$$T_1(x, \zeta) = \tilde{T}(\xi) , \tag{122}$$

where $\xi = \zeta \, x^\alpha$ for some value of α. Substitution of (122) into (120) shows that $\alpha = -1/3$ must hold, and consequently the solution can be found as

$$T(x, \zeta) = T_1(x, \zeta) = C \int_0^{\frac{\zeta}{\sqrt[3]{x}}} e^{-\frac{2}{9}s^3} ds , \tag{123}$$

where C is given by

$$C = \left(\int_0^\infty e^{-\frac{2}{9}s^3} ds \right)^{-1} . \tag{124}$$

We can proceed in a completely analogous way to derive second and higher order (in ε) terms in this asymptotic solution. The second order term is given by

$$T_2(\zeta, \xi) = -\frac{C\zeta}{10} \left(\int_\xi^\infty e^{-\frac{2}{9}s^3} ds + \xi e^{-\frac{2}{9}\xi^3} \right) . \tag{125}$$

The total solution for the temperature in Ω_0 is now

$$T(x, \zeta) = T_1(x, \zeta) + \varepsilon T_2(x, \zeta) + O(\varepsilon^2) . \tag{126}$$

We compare the asymptotic solution of (126) with a numerical solution obtained by means of a finite difference method. In Table 1 the results are shown for the case that $\kappa = 0.01$. The results for $T(x, z)$ at $x = 1$ are shown (in dimensionful variables, $x = 1$ corresponds to $x = 6 \cdot 10^{-2}$m). In this table, T_1^{as}, T_2^{as}, ΔT_1^{as} and ΔT_2^{as} are defined by

$$T_1^{as}(x, z) = T_1 \left(x, \frac{1-z}{\varepsilon} \right) ,$$
$$T_2^{as}(x, z) = (T_1 + \varepsilon T_2) \left(x, \frac{1-z}{\varepsilon} \right) ,$$
$$\Delta T_1^{as} = \frac{T_1^{as} - T^{num}}{T^{num}},$$
$$\Delta T_2^{as} = \frac{T_2^{as} - T^{num}}{T^{num}}. \tag{127}$$

From Table 1 it follows that the asymptotic solution and the numerical solution are in good agreement with each other, despite the fact that $\varepsilon = \sqrt[3]{\kappa} = 0.21$, which is not really very small.

Next, we consider the:

Table 1. Comparison between asymptotic and numerical results at $x = 1$

z value	Asympt. sol.		Num. sol.	Relative difference	
	T_1^{as}	T_2^{as}	T^{num}	ΔT_1^{as}	ΔT_2^{as}
0.0	1.000	1.000	1.000	$5.47 \cdot 10^{-7}$	$5.47 \cdot 10^{-7}$
0.1	1.000	1.000	1.000	$5.42 \cdot 10^{-7}$	$5.18 \cdot 10^{-7}$
0.2	1.000	1.000	1.000	$1.47 \cdot 10^{-5}$	$1.23 \cdot 10^{-5}$
0.3	1.000	1.000	1.000	$2.09 \cdot 10^{-4}$	$1.31 \cdot 10^{-4}$
0.4	0.999	0.998	0.997	$1.59 \cdot 10^{-3}$	$5.98 \cdot 10^{-4}$
0.5	0.990	0.985	0.984	$6.71 \cdot 10^{-3}$	$1.23 \cdot 10^{-3}$
0.6	0.946	0.932	0.930	$1.74 \cdot 10^{-2}$	$2.03 \cdot 10^{-3}$
0.7	0.824	0.803	0.799	$3.15 \cdot 10^{-2}$	$5.41 \cdot 10^{-3}$
0.8	0.603	0.585	0.578	$4.42 \cdot 10^{-2}$	$1.22 \cdot 10^{-2}$
0.9	0.313	0.303	0.297	$5.28 \cdot 10^{-2}$	$1.94 \cdot 10^{-2}$
1.0	0.000	0.000	0.000		

Flow front region

$$\underline{(x, z) \in \Omega_f,} \qquad \text{where} \quad \Omega_f = \{(x, z) \mid x_f < x < x_{f0}, \ -h < z < h \},$$

with $x_{f0} = x_f + R_f(0, t) - R_f(h, t) = R_f(0, t) - R_n$ (see Fig. 16).
In this region, $x - x_f$ and z are of the same order of magnitude, implying the choice $L = h$, and moreover also $(v_x - V_f)$ and v_z are of the same order. Therefore, we introduce new variables $\tilde{x}, \tilde{z}$ and $\tilde{t}$ as

$$\tilde{x} = \frac{x - x_f}{h} , \qquad \tilde{z} = \frac{z}{h} , \qquad \tilde{t} = \frac{V_f}{h} \, t , \tag{128}$$

write the velocity as (note that u and w are known from the preceding zeroth order velocity problem)

$$\mathbf{v} = V_f \left[\left(\frac{3}{2}(1 - \tilde{z}^2) + \tilde{u}(\tilde{x}, \tilde{z}) \right) \mathbf{e}_x + \tilde{w}(\tilde{x}, \tilde{z}) \mathbf{e}_z \right] , \tag{129}$$

and consider the temperature in the *moving* frame $(\tilde{x}, \tilde{z})$, i.e.

$$\frac{T(x, z, t) - T_w}{T_i - T_w} = \tilde{T}(\tilde{x}, \tilde{z}, \tilde{t}) . \tag{130}$$

With all this, the convective-diffusive heat equation (106) turns into

$$\frac{\partial \tilde{T}}{\partial \tilde{t}} + \left(\frac{1}{2}(1 - 3\tilde{z}^2) + \tilde{u} \right) \frac{\partial \tilde{T}}{\partial \tilde{x}} + \tilde{w} \frac{\partial \tilde{T}}{\partial \tilde{z}} = \tilde{\kappa} \triangle \tilde{T} , \tag{131}$$

where

$$\tilde{\kappa} = \frac{\kappa}{V_f h} = \frac{h}{R}\hat{\kappa} \; . \tag{132}$$

Since $\hat{\kappa}$ itself is already small, we thus have $\tilde{\kappa} \ll 1$, and therefore we may neglect the diffusive term in (131). Moreover, because

$$\tilde{\mathbf{v}} = \left(\frac{1}{2}(1 - 3\tilde{z}^2) + \tilde{u}\right)\mathbf{e}_x + \tilde{w}\mathbf{e}_z \; , \tag{133}$$

is precisely the velocity of a material particle *with respect to the flow front*, we may write

$$\frac{\partial \tilde{T}}{\partial \tilde{t}} + (\tilde{\mathbf{v}} \cdot \nabla \tilde{T}) = 0 \; , \tag{134}$$

expressing that the change in time of $\tilde{T}$ is purely due to convection. Consequently, the temperature of each material particle moving in the front region remains equal to the temperature with which it enters this region. Because (from the beginning of the filling of the cavity on) this temperature is always equal to T_i, this implies that the temperature in the whole front region will be uniform and equal to T_i. However, this solution then leads to two evident contradictions:

- the temperature at the tips of the flow region ($\tilde{z} = \pm 1$) should be T_w instead of T_i ($\Rightarrow \quad \tilde{T} = 0$, at $\tilde{z} = \pm 1$);
- the temperature in the boundary layer in Ω_0 directly behind the straight flow front boundary $x = x_f$ of Ω_f is smaller than T_i, causing the temperature across this boundary to become discontinuous.

From these discrepancies we conclude that there should also exist a boundary layer within Ω_f, extending behind Ω_f, and continuously merging into the boundary layer in Ω_0. In this boundary layer, the diffusion must again be taken into account. However, as $\tilde{\kappa} \ll \hat{\kappa}$, the boundary layer in Ω_f will be much ($O(h/R)$) narrower than the one in Ω_0. A sketch of the expected temperature distribution in the cavity at a certain position of the flow front is given in Fig. 16. The analysis of the latter boundary layer can be done in a way analogous to the one dealt with in the preceding subsection. However, at this stage in the project, this point is still under study. In fact, this is the stage in the project reached by now. Knowing the zeroth order unperturbed solution, we hope to proceed with a study of the perturbed problem. The perturbation will be assumed due to an initial asymmetry in the flow front. We will examine how this asymmetry influences the flow. This influence will be most manifest in the boundary layers. Our main focus will be the evolution in time of the (asymmetric) shape of the flow front.
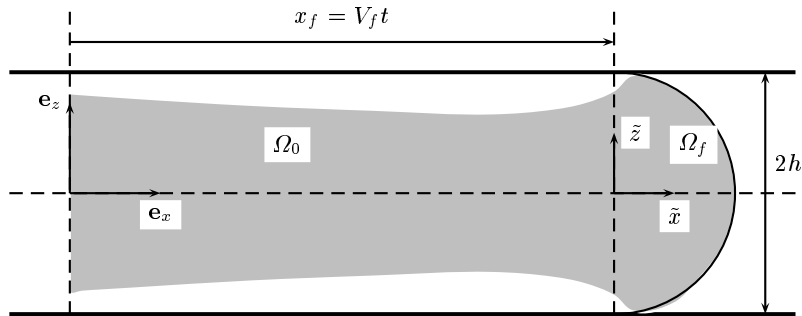
Fig. 16. Sketch of the temperature distribution in the cavity, behind and in the flow front region; in the gray part the temperature is T_i.

4   Closing Remarks

In this contribution, a survey is presented of the research on polymers performed by a unit of the mathematics faculty of Eindhoven University of Technology (EUT) during the years 1995 to 2000. Special attention is given to the mathematical modelling of industrial processes for polymers, and to the analytical and numerical evaluation of the models thus obtained. In Sect 2, we presented some results of two projects investigating the (in)stability of the extrusion process for polymer melts. The instability considered here is the so called spurt phenomenon. A 3-dimensional model describes spurt either as a sudden huge increase in flow rate at a slight increase in pressure or as the onset of persistent oscillations in both the pressure and the flow rate. A discrete stick-slip model describes spurt in terms of relaxation oscillations in the pressure and the flow rate. The latter model is at one hand mathematically simple, but on the other hand it yields a good correspondence, both qualitatively and quantitatively, with existing experimental results.

In Sect 3, injection moulding between two parallel plates is considered. A general model for the mechanical (flow, pressure, stresses) and thermal features (temperature, heat flux) of this process is presented. A project (still in an initial state) on the instability ('wobbling') of the free flow front is discussed. Based on the expectation that the wobbling could be driven by asymmetric temperature distributions, a possible solution for this stability problem is presented. Hence, the source for the wobbling of the front is sought in first instance in thermal effects (and not in elasticity effects).

To close the survey of 1995-2000, we would like to indicate some future projects within our unit. First there is the PhD-project of Gramberg, already mentioned above. This project runs till the end of 2002. We are now focussing

on analytical methods, but in the second part of the project also numerical simulations will come into sight. Secondly, there is the PhD-project of Smolders on the thermoviscoelastic modelling of injection moulding (mentioned in Sect. 3.1). Besides a complete numerical simulation of the process, this project especially aims at calculations of residual stresses and deformations, specifically in connection with birefringence (e.g. in compact discs). This project runs till the end of 2003. Finally, we mention the PhD-project of Gunawan on the morphology of polymeric blends (see Sect. 1.3). This project is especially concerned with the disintegration of polymer threads in a polymer matrix, and with the material features of the resulting polymer blend. This project runs till the end of 2004.

All these projects are supervised by Molenaar and Van de Ven, and are in cooperation with industrial companies as DSM, DOW and Axxicon.

References

1. Aarts, A.C.T. (1997) Analysis of the Flow Instabilities in the Extrusion of Polymeric Melts. Ph.D.Thesis, Eindhoven University of Technology
2. Doelder, C.F.J. den. (1999) Design and Implementation of Polymeric Melt Fracture Models. Ph.D.Thesis, Eindhoven University of Technology
3. Aarts, A.C.T., and Ven, A.A.F. van de. (1995) Transient Behaviour and Stability Points of the Poiseuille Flow of a KBKZ-fluid. J. Eng. Math., **29**, 371-392
4. Doelder, C.F.J.den, Koopmans, R.J., Molenaar, J., Ven, A.A.F. van de. (1998) Comparison of Wall Slip and Constitutive Instability Spurt Models. J. Non-Newtonian Fluid Mech. **75**, 25-41
5. Malkus,D.S., Nohel, J.A., Plohr, B.J. (1991) Analysis of new phenomena in shear flow of non-Newtonian fluids. SIAM Journal on Applied Mathematics **51**, 899-929
6. Aarts, A.C.T., Ven, A.A.F.van de. (1999) The Occurrence of Periodic Distortions in the Extrusion of Polymeric Melts. Continuum Mechanics and Thermodynamics, **11**, 113-139
7. Tanner, R.I. (1988) Engineering Rheology. Clarendon Press, Oxford
8. Ven, A.A.F. van de. (1999) Comparing Stick and Slip Models for Spurt in the Extrusion of Polymeric Melts. In: Progress in Industrial Mathematics at ECMI98, eds: L. Ackeryd, J. Bergh, P. Brenner, R. Petterson. Proceedings of 10th ECMI-Conference, ECMI 98, Göteborg (pp. 154-162). Teubner, Stuttgart
9. Greenberg, J.M., Demay, Y. (1994) A Simple Model of the Melt Fracture Instability, European Journal of Applied Mathematics **5**, 337-358
10. Doelder, C.F.J. den, Koopmans, R.J., Molenaar, J. (1998) Quantitative Modelling of HDPE Spurt Experiments Using Wall Slip and Generalised Newtonian Flow, J. Non-Newtonian Fluid Mech. **79**, 503-514.
11. Kennedy, P. (1995) Flow analysis in injection molds. Hanser Publishers, Munich Vienna New York
12. Vroonhoven, J.C.W., Kuijpers, W.J.J. (1990) A Free-boundary Problem for Viscous Fluid Flow in Injection Moulding. J. Eng. Math. **24**, 151-165

Index

asymptotic solution, 46

Bagley correction, 36
balance of energy, 39
balance of linear momentum, 11
balance of mass, 8, 26
birefringence, 50
blow moulding, 5
boundary layer, 45, 48

cable coating, 5
compressibility, 8, 18, 37
– isothermal, 40
compression, 15
conformal mapping, 43
constitutive equation
– compressibility law, 8, 26
– for ρ, 39
– heat flux, 39
– – Fourier's law, 39
– stress, 9, 39
– – generalised Newtonian, 36
– – JSO, 10, 15
– – KBKZ, 10, 11, 14
– – Leonov, 39

density, 8, 38
die swell, 5

equation of continuity, 38
equation of motion, 8, 9, 26, 38
extrusion, 1, 2, 6, 7, 15, 17

fiber spinning, 5
filling phase, 37, 38
flow
– capillary, 27
– classical, 12, 19, 20, 26, 27, 29, 32
– compression flow, 8
– curve, 21, 22
– front, 47
– fully developed, 44
– incompressible, 8, 26
– piston-driven, 10, 15
– pressure-driven, 10

– profile, 26
– shear dominated, 8, 26
– spurt, 23, 26, 27, 29, 31
– subcritical, 12, 20
– supercritical, 12, 14, 19, 20, 22
– transient, 25
flow front
– shape of, 43
fluid
– compressible, 40
– generalised Newtonian, 37, 39
– incompressible, 42
– Newtonian, 27, 42
– thermoviscoelastic, 37
free boundary, 43
front, 38
– free boundary of, 37, 41
– free surface, 38
– motion, 37

Gibbs law, 40

heat capacity, 40
heat flux, 39
– heat conduction coefficient, 39
– heat diffusion equation, 45
Hilbert problem, 43
hysteresis, 10, 12, 13

incompressibility conditi, 8
incompressibility condition, 40
injection moulding, 3, 37, 41, 49
instability
– constitutive, 7, 24
– extrusion, 6
– flow front, 3, 41
– flow instabilities, 10
– in extrusion, 25, 34
– spurt, 24, 49
– thermally induced, 37
internal energy density, 39

latency, 13
– phase, 14

melt fracture, 25
modulus
– bulk, 8
– compression, 8
– shear, 15
morphology, 4

Newtonian
– phase, 14
– viscous term, 10
no-slip, 8–10, 17, 26, 40

oscillations
– persistent, 22, 23

polymer blend, 4, 50
pressure, 7, 9, 17, 21, 22, 26, 38
pressure gradient, 9–11, 26

rate-of-deformation, 9, 39
relaxation oscillations, 3, 25, 26, 29, 32, 34
relaxation rate, 11, 25

sag, 5
shape memory, 10, 12, 13, 24, 27
shear rate, 17, 39
shear strain, 11
shear thinning, 37
slip, 29
– law, 29
– model, 29
– velocity, 29
slip parameter, 15
solvent viscosity, 9, 11
spurt, 10, 12, 15, 20, 25, 26, 34

– flow, 20
– layer, 13, 20
– phase, 14
– zone, 25–27
steady state, 11, 18, 20
stick-slip, 3, 29
stress
– elastic part, 9, 15
– extra stress tensor, 9, 39
– first normal stress difference, 14, 16
– residual stresses, 3, 37, 50
– second normal stress difference, 16
– shear stress, 10, 11, 19, 26
– total stress tensor, 8, 38
switch curve, 28

temperature, 37, 38, 44, 46, 48
thermal
– convection, 48
– diffusion, 45, 48
– diffusion constant, 43
– effects, 37
– expansion, 40
– fields, 37
– shrinkage, 3

velocity, 8, 38, 41, 47
– gradient, 11–13, 17, 18, 20
– profile, 12, 19
viscosity, 27, 39
– Newtonian viscosity, 19
– shear viscosity, 19
– temperature dependent, 42
volumetric flow rate, 7, 8, 10, 11, 17, 20, 22, 26